



HAL
open science

WALLABY Pre-Pilot and Pilot Survey: the Tully Fisher Relation in Eridanus, Hydra, Norma and NGC4636 fields

Hélène M. Courtois, Khaled Said, Jeremy Mould, T. H. Jarrett, Daniel Pomarède, Tobias Westmeier, Lister Staveley-Smith, Alexandra Dupuy, Tao Hong, Daniel Guinet, et al.

► To cite this version:

Hélène M. Courtois, Khaled Said, Jeremy Mould, T. H. Jarrett, Daniel Pomarède, et al.. WALLABY Pre-Pilot and Pilot Survey: the Tully Fisher Relation in Eridanus, Hydra, Norma and NGC4636 fields. *Monthly Notices of the Royal Astronomical Society*, 2023, 519, pp.4589-4607. 10.1093/mnras/stac3246 . insu-03863222

HAL Id: insu-03863222

<https://insu.hal.science/insu-03863222>

Submitted on 12 Jul 2023

HAL is a multi-disciplinary open access archive for the deposit and dissemination of scientific research documents, whether they are published or not. The documents may come from teaching and research institutions in France or abroad, or from public or private research centers.

L'archive ouverte pluridisciplinaire **HAL**, est destinée au dépôt et à la diffusion de documents scientifiques de niveau recherche, publiés ou non, émanant des établissements d'enseignement et de recherche français ou étrangers, des laboratoires publics ou privés.

WALLABY pre-pilot and pilot survey: The Tully Fisher relation in Eridanus, Hydra, Norma, and NGC4636 fields

Hélène M. Courtois ^{1,★}, Khaled Said ², Jeremy Mould,³ T. H. Jarrett ⁴, Daniel Pomarède,⁵ Tobias Westmeier ^{6,7}, Lister Staveley-Smith ^{6,7}, Alexandra Dupuy ^{1,8}, Tao Hong,⁹ Daniel Guinet,¹ Cullan Howlett ², Nathan Deg ¹⁰, Bi-Qing For ⁶, Dane Kleiner ¹¹, Bärbel Koribalski ^{12,13}, Karen Lee-Waddell ^{6,14}, Jonghwan Rhee,^{6,7} Kristine Spekkens,¹⁵ Jing Wang,¹⁶ O. I. Wong ^{6,7,14}, Frank Bigiel,¹⁷ Albert Bosma ¹⁸, Matthew Colless ¹⁹, Tamara Davis ², Benne Holwerda ²⁰, Igor Karachentsev,²¹ Renée C. Kraan-Korteweg,⁴ Kristen B. W. McQuinn,²² Gerhardt Meurer,⁶ Danail Obreschkow ^{6,7} and Edward Taylor³

Affiliations are listed at the end of the paper

Accepted 2022 October 14. Received 2022 September 19; in original form 2022 January 27

ABSTRACT

The WALLABY pilot survey has been conducted using the Australian SKA Pathfinder (ASKAP). The integrated 21-cm H I line spectra are formed in a very different manner compared to usual single-dish spectra Tully–Fisher measurements. It is thus extremely important to ensure that slight differences (e.g. biases due to missing flux) are quantified and understood in order to maximise the use of the large amount of data becoming available soon. This article is based on four fields for which the data are scientifically interesting by themselves. The pilot data discussed here consist of 614 galaxy spectra at a rest wavelength of 21 cm. Of these spectra, 472 are of high enough quality to be used to potentially derive distances using the Tully–Fisher relation. We further restrict the sample to the 251 galaxies whose inclination is sufficiently close to edge-on. For these, we derive Tully–Fisher distances using the deprojected WALLABY velocity widths combined with infrared (*WISE* W1) magnitudes. The resulting Tully–Fisher distances for the Eridanus, Hydra, Norma, and NGC4636 clusters are 21.5, 53.5, 69.4, and 23.0 Mpc, respectively, with uncertainties of 5–10 per cent, which are better or equivalent to the ones obtained in studies using data obtained with giant single dish telescopes. The pilot survey data show the benefits of WALLABY over previous giant single-dish telescope surveys. WALLABY is expected to detect around half a million galaxies with a mean redshift of $z = 0.05$ (200 Mpc). This study suggests that about 200 000 Tully–Fisher distances might result from the survey.

Key words: surveys – galaxies: distances and redshifts – large-scale structure of Universe.

1 INTRODUCTION

Tully & Fisher (1977) discovered a relation (the Tully–Fisher relation: TFR) between the extensive properties of disc galaxies (mass, luminosity, and radius) and their rotation velocity, which can be derived from the velocity width of their neutral hydrogen 21-cm spectra. If galaxy surface brightness, stellar mass, and mass to light ratio are functions of halo mass, the virial theorem leads one to expect a luminosity–rotation velocity relation. As the TFR relates distance-independent and distance-dependent quantities, it can be used to measure galaxy distances and peculiar velocities. Developments in understanding galaxy scaling relations are reviewed by Mould (2020). The TFR is also reproduced in dark matter simulations, when subgrid physics is added to follow the baryons (e.g. Springel et al. 2018), so it can, therefore, also be used to further probe the astrophysics of galaxy formation.

The Widefield ASKAP *L*-band Legacy All-sky Blind Survey (WALLABY) pre-pilot and pilot phase 1 survey is an observational study of four fields with the Australian Square Kilometer Array Pathfinder (ASKAP) telescope. The pilot observations are a precursor to the full WALLABY survey, a blind neutral hydrogen survey of the Southern hemisphere (Koribalski et al. 2020) which is scheduled to begin in 2022. The pilot data has already been used to study H I content of galaxies in groups (For et al. 2021), discover dark clouds in the vicinity of galaxies (Wong et al. 2021), and study the diversity of ram pressure stripping of H I gas in galaxies in the Hydra cluster (Wang et al. 2021).

The raw ASKAP visibilities from the WALLABY observations are processed and reduced using ASKAPsoft. The processed data products are available on CASDA. The data are first released to the WALLABY team for analysis, and, once published, available to the wider community. A mosaic of individual footprints is then made to produce the final full sensitivity cubes which are run through the SoFiA pipeline. SoFiA is a 3D source finding and parametrization software package (Serra et al. 2015; Westmeier et al.

* E-mail: h.courtois@ip2i.in2p3.fr

2021) which, amongst many other outputs, produces a 1-dimensional spectrum by spatially integrating all emission within its mask. The measured HI linewidth is a measure of the galaxy projected rotation velocity.

In this article, we explore the infrared TFR, by combining WALLABY pilot HI spectra with photometric data using *WISE* W1 band infrared fluxes. Infrared wavelengths have the advantage of markedly lower extinction of galaxy radiation by dust (Aaronson, Huchra & Mould 1979). It is now well known that using infrared data provides a tighter TFR than using optical bands (Sorice et al. 2013; Neill et al. 2014; Kourkchi et al. 2020b). The measured galaxy distances can be used to: measure the expansion rate through determination of the Hubble constant (Kourkchi et al. 2020b); test the Λ CDM cosmological model using measurements of the bulk flow (Hoffman, Courtois & Tully 2015; Hong et al. 2019); compute systematics in the SNIa Hubble constant determination (Peterson et al. 2022). Another question that measurements of non-Hubble flows can address is the quantity of matter needed in specific regions such as the Great Attractor in order to explain gravitationally-induced motions, with the aim of reconciling with observed baryonic matter distribution (Said et al. 2020; Thévenot et al. 2020).

A major benefit of the WALLABY survey is its higher sensitivity compared to previous southern surveys used for Tully–Fisher distances – for example, the HI Parkes All-Sky Survey (HIPASS; Koribalski et al. 2004; Meyer et al. 2004). It also has higher survey speed than northern single-dish telescopes, previously used to conduct HI surveys (Haynes et al. 2018); thanks to its wide (30 deg^2) instantaneous field of view, thus enabling to construct larger galaxy samples. Other advantages are the location of ASKAP at a site that is free from terrestrial radio frequency interference and its high-angular resolution, which allows detailed morphological and dynamical studies. Although angular resolution is not important for this TFR study, it does lessen the probability of beam confusion and will allow future dynamical measurements of inclination.

All-sky infrared surveys provide complementary data for large samples of galaxies with a depth, resolution, and photometric accuracy suitable for TFR studies. Examples include the 2MASS Tully–Fisher (2MTF) survey of 2062 galaxies (Hong et al. 2019) and the *WISE* Tully–Fisher study of Lagattuta et al. (2013). Currently, the largest Tully–Fisher samples are of the order of 10 000 galaxies (Kourkchi et al. 2020b), while WALLABY is planned to triple or more this latter number in the next few years (Koribalski et al. 2020). The Meerkat SKA precursor located in South Africa is also used to successfully derive baryonic Tully–Fisher galaxy distances (Ponomareva et al. 2021).

Galaxy distances are key to the objective of the CosmicFlows (CF) project (Tully, Courtois & Sorice 2016), which is to improve the cosmography of the nearby universe including the location and mass measurement of the largest attractors. Distances are used to compute velocity deviations from the Hubble cosmic expansion, which are assumed to arise from the large-scale gravitational field. This can only be realized with very accurate distances. The CF project started in 2006, and will shortly publish its fourth generation catalogue containing about 45 000 accurate determinations of galaxy distances.

In this paper, we describe the pre-pilot and phase 1 pilot WALLABY surveys from which our HI data is drawn, and present optical identifications of the detected sourced at 21 cm (Section 2); we form TFRs by using accurate photometry in the *WISE* W1 bandpass (Section 3). Finally, we show how the WALLABY Survey can add to the CF data base for future studies of large-scale structure.

2 WALLABY PRE-PILOT AND PILOT SURVEY

WALLABY is an extragalactic all-sky HI survey with the ASKAP telescope, which consists of $36 \times 12 \text{ m}$ dishes with baselines ranging from 22 m to 6 km (Hotan et al. 2021). It is equipped with phased array feeds with a field-of-view of about 30 deg^2 at 1.4 GHz. The frequency coverage of ASKAP is from 0.7 to 1.8 GHz with an instantaneous bandwidth of 288 MHz. Its spectral resolution of 18.5 kHz translates into a velocity resolution of 4 km s^{-1} at redshift zero.

For the WALLABY pilot surveys, a bandwidth of 144 MHz covering the frequency range of 1295.5 to 1439.5 MHz was processed and imaged. This corresponds to redshifts $z < 0.096$. All baselines, including the 6 km baselines, were calibrated. However, the current WALLABY images only include baselines up to 2 km, resulting in an angular resolution of 30 arcsec. The nominal RMS noise level is approximately 1.6 mJy after two footprints, each of duration 8 h, are combined. We refer the reader to Koribalski et al. (2020) for more details about the WALLABY survey.

2.1 Radio and photometry data measurements

The pre-pilot and pilot phase 1 survey resulted in coverage of the NGC4636 group, the Eridanus super group, the Hydra I cluster, and the Norma cluster surrounds (the actual Norma cluster is excluded from this study due to strong residual radio continuum emission). Sources were catalogued using the SoFIA source finding pipeline (Serra et al. 2015; Westmeier et al. 2021). Detections were linked across a spatial and spectral radius of two pixels with a minimum size requirement for reliable source identification of five spatial pixels and eight spectral channels. SoFIA’s reliability filter was then applied to remove all detections with a reliability below 0.8, using a Gaussian kernel density estimator of size 0.35 times the covariance. All remaining sources were then parametrized, assuming a restoring beam size of 30 arcsec for all integrated flux measurements. The source detection details slightly vary between the four different fields – details will be provided in the upcoming paper accompanying the first public data release of phase 1 pilot data (Westmeier et al. 2022).

The pre-pilot field containing the Eridanus super group was observed with two interleaving footprints (A and B) with an offset of 38 arcmin, and rotated by a position angle of 45 deg relative to a standard ASKAP footprint. The Norma, Hydra, and NGC4636 pilot observations were of two adjacent 30 deg^2 overlapping tiles (1 and 2), with the tile centres separated by 5.4 deg. Each tile consisted of two slightly offset footprints observed for 8 h. Therefore, each 1-D HI spectrum has an effective integration time of 16 h. The centres of the footprints are given in Table 1.

2.2 Comparison of velocity width measurement algorithms

SoFiA provides approximate linewidths for all galaxies that it finds in WALLABY cubes. However, to improve robustness, accuracy, reliability and compatibility with previous measurements, we also compute linewidths using the CF methodology and make a detailed comparison with the SoFiA estimates.

The CF linewidth W_{m50} , is measured at the flux level that is 50 per cent of the mean flux, averaged in channels within the wavelength range enclosing 90 per cent of the total integrated flux (Courtois et al. 2011a; Courtois, Tully & Héraudeau 2011b). It is followed by a correction for redshift and instrumental broadening: $W_{m50}^{\text{corr}} = (W_{m50} - 2\Delta v\lambda)/(1+z)$, where z is the redshift in the CMB frame, Δv is the smoothed spectral resolution, and $\lambda = 0.25$ is an empirically determined constant (Courtois et al. 2009). The observed line width

Table 1. Table of J2000 coordinates pointings of the WALLABY pre-pilot and pilot phase 1 survey fields.

| Footprint | Field centre (J2000) | |
|------------|----------------------|--------------|
| | RA | DEC |
| Eridanus A | 03:39:30.000 | -22:23:00.00 |
| Eridanus B | 03:36:44.520 | -22:37:54.69 |
| Hydra-1A | 10:15:47.844 | -27:22:27.66 |
| Hydra-1B | 10:17:49.958 | -27:49:24.30 |
| Hydra-2A | 10:39:24.238 | -27:22:27.66 |
| Hydra-2B | 10:41:26.352 | -27:49:24.30 |
| NGC4636-1A | 12:38:02.328 | -00:26:59.95 |
| NGC4636-1B | 12:39:50.337 | -00:53:59.85 |
| NGC4636-2A | 12:38:02.729 | +04:56:58.64 |
| NGC4636-2B | 12:39:51.059 | +04:29:58.13 |
| Norma-1A | 16:16:30.928 | -59:27:41.88 |
| Norma-1B | 16:20:06.332 | -59:54:30.90 |
| Norma-2A | 16:55:26.063 | -59:27:41.88 |
| Norma-2B | 16:59:01.467 | -59:54:30.90 |

was also adjusted by separating out the broadening from turbulent motions and offsets to produce an approximation to $2V_{\max}$, where $V_{\max} = W_{\text{mx}}/2$ correspond to the rotation rate over the main body of a galaxy. Tully & Fouqué (1985) define the parameter W_{mx} as:

$$W_{\text{mx}}^2 = W_{\text{m50}}^{\text{corr},2} + W_{\text{t,m50}}^2 \left[1 - 2e^{-(W_{\text{m50}}^{\text{corr}}/W_{\text{c,m50}})^2} \right] - 2W_{\text{m50}}^{\text{corr}} W_{\text{t,m50}} \left[1 - e^{-(W_{\text{m50}}^{\text{corr}}/W_{\text{c,m50}})^2} \right]. \quad (1)$$

The parameters $W_{\text{c,m50}} = 100 \text{ km s}^{-1}$ and $W_{\text{t,m50}} = 9 \text{ km s}^{-1}$ are set following tests conducted in Courtois et al. (2009), and characterize, respectively, the transition from boxcar to Gaussian intrinsic profiles, and the turbulent broadening for the observed linewidth considered. It is then related to the rotation rate V_{\max} by:

$$V_{\max} = \frac{W_{\text{mx}}}{2 \sin(i)}, \quad (2)$$

where i is the inclination of the galaxy from face-on relative to the observer.

Details regarding the W_{m50} and W_{mx} line width parameters and comparisons with alternatives are discussed in Courtois et al. (2009). A comparison of the CF and SoFiA linewidth measurements in the Norma field is shown in Fig. 1.

We make a further comparison with velocity widths derived using the method described by Said et al. (2016, hereafter S16). This algorithm requires prior knowledge of the left and right horns which is currently done manually, and returns the linewidth measured at 50 per cent of the mean flux and its associated uncertainty. In this paper, we compare the CF linewidth with the S16 linewidth measured at 50 per cent of the mean flux, as shown in Fig. 2.

We use the relative error between pairs of measurements to quantitatively check for any large discrepancies between 50 per cent widths measured with the CF algorithm and widths measured at 50 per cent of the mean flux with the S16 algorithm. We used the pairwise relative error of the form:

$$\varepsilon = \frac{W_{\text{m50}}^{\text{CF}} - W_{\text{m50}}^{\text{S16}}}{\sqrt{(eW_{\text{m50}}^{\text{CF}})^2 + eW_{\text{m50}}^{\text{S16}})^2}}, \quad (3)$$

where $W_{\text{m50}}^{\text{CF}}$, $W_{\text{m50}}^{\text{S16}}$, $eW_{\text{m50}}^{\text{CF}}$, and $eW_{\text{m50}}^{\text{S16}}$ are the 50 per cent widths measurements from CF and S16 algorithms and their associated statistical uncertainties, respectively. Values of ε for all galaxies are within the distribution of a Gaussian with a mean of zero and a

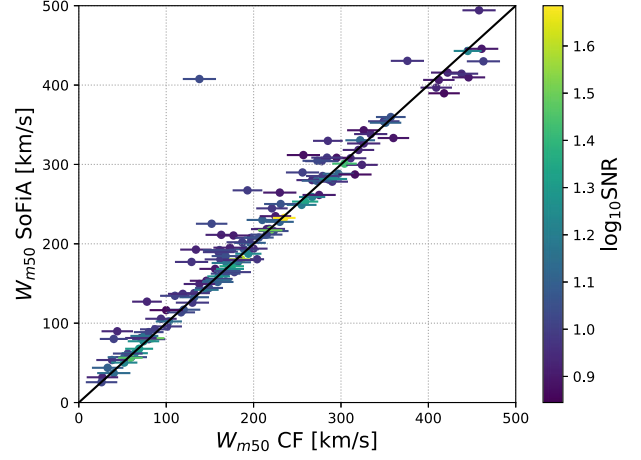


Figure 1. Linewidths W_{m50} in the Norma field as measured by the CosmicFlows (CF) algorithm compared with the automatic measurements of SoFiA, colour-coded by S/N ratio. The plot only includes spectra with an error on W_{m50} less or equal to 20 km s^{-1} . Two further spectra with low S/N ratio, where the linewidth difference exceeds 100 km s^{-1} , are excluded from the plot.

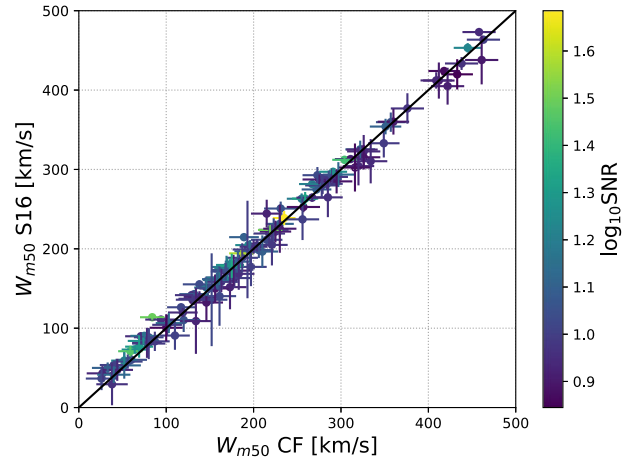


Figure 2. Comparison of 50 per cent linewidths in the Norma field measured with the CF algorithm and linewidths measured at 50 per cent of the mean flux using the S16 algorithm (Said et al. 2016). Only measurements of spectra with an adequate quality are displayed (error on W_{m50} less or equal to 20 km s^{-1}). This comparison displays a typical scatter at 20 km s^{-1} .

standard deviation of unity. Table 2 lists all discrepant measurements with $|\varepsilon| > 1.0$.

Following the CF collaboration, the signal-to-noise ratio is calculated by taking the mean flux density across all channels in excess of 95 per cent of the peak, and dividing it by the noise level in the spectrum as measured outside of the H I line (Courtois & Tully 2015).

The error on the linewidth e_W in km s^{-1} , follows the empirical relation from (Courtois et al. 2009):

$$\begin{aligned} \text{SNR} \geq 17 & \quad e_W = 8 \text{ km s}^{-1}; \\ 2 < \text{SNR} < 17 & \quad e_W = 21.6 - 0.8 \times \text{SNR km s}^{-1}; \\ \text{SNR} \leq 2 & \quad e_W = 70 - 25 \times \text{SNR km s}^{-1}, \end{aligned} \quad (4)$$

where SNR is the signal-to-noise ratio. CF has shown that an H I spectrum is considered adequate for estimating galaxy distance through the TFR if the error on W_{m50} is less or equal to 20 km s^{-1} . As seen in Fig. 2, this threshold is confirmed once again by this study.

Table 2. All galaxies with pairwise relative error $|\epsilon| > 1.0$, between the CF and S16 algorithms.

| name | PGC | W_{m50} | $e_{W_{m50}}$ | W_{m50}^{S16} | $e_{W_{m50}}^{S16}$ | ϵ |
|----------------|-------|-----------|---------------|-----------------|---------------------|------------|
| J102439-244547 | 30532 | 94 | 18 | 112 | 2 | -1.0177 |
| J102447-264054 | 30545 | 271 | 17 | 322 | 13 | -2.4078 |
| J103442-283406 | 31296 | 247 | 15 | 263 | 4 | -1.0149 |
| J103726-261843 | 31557 | 199 | 18 | 224 | 2 | -1.3854 |
| J104127-275119 | 31842 | 99 | 19 | 119 | 5 | -1.0091 |
| J104142-284653 | 31855 | 107 | 15 | 128 | 7 | -1.2566 |
| J104513-262755 | | 50 | 17 | 74 | 6 | -1.3571 |
| J104905-292232 | 32361 | 117 | 17 | 142 | 3 | -1.4259 |
| J163452-603705 | 58536 | 189 | 17 | 215 | 1 | -1.5087 |
| J164359-600237 | | 215 | 18 | 244 | 17 | -1.1702 |
| J165105-585918 | 59112 | 84 | 14 | 114 | 3 | -2.0721 |
| J165145-590915 | | 71 | 18 | 90 | 5 | -1.0111 |

In summary for the three algorithms for W_{m50} : (1) SoFiA is automated, but sometimes gives discrepant measurements for low-SNR spectra (see Fig. 1). It also has a dispersion of about 50 km s^{-1} , which is too high for Tully–Fisher purposes (Courtois et al. 2009). (2) The adopted CF algorithm is semi-automated with a final inspection by eye of the fit. In some cases (six spectra, corresponding to about 1 per cent of all spectra in the pilot survey), a fit was not possible. (3) The S16 algorithm requires a starting value for W_{m50} (that can be provided by SoFiA), but appears to provide a measurement which is within the 20 km s^{-1} error limit on W_{m50} that we impose for TFR studies. Therefore the WALLABY survey data will be treated by all three algorithms. The comparison of the results per individual galaxy will allow to identify the difficult spectra that require close inspection.

Details of all the galaxies selected at 21 cm for this TF study are listed in Appendix A.

2.3 Comparison with previous single-dish velocity width measurements

In this section, we check whether there are any differences between single-dish and multidish spectroscopic data, that would affect the quality of the derived Tully–Fisher distances with systematic errors.

Fortunately, there is a sufficient overlap with existing data to check consistency between pilot WALLABY and published single-dish velocity widths as compiled in the Extragalactic Distance Database (Courtois & Tully 2015). This comparison is shown in Fig. 3 for the galaxies in common. There is no significant difference when comparing the WALLABY W_{mx} values with those measured from single-dish data, with most agreeing within the 20 km s^{-1} limit. The discrepant data comes from wrong width measurements from low-S/N ratio Arecibo spectra and measurements of WALLABY spectra containing residual continuum from strong nearby sources outside the field and, therefore, not cleaned. This comparison is an excellent external robustness assessment of the capability of WALLABY to deliver satisfactory HI data to the community. It also demonstrates that the exposure time used for the Phase 1 Pilot Survey can be considered as the guideline for the upcoming large WALLABY survey.

2.4 WISE photometry

The *Wide-field Infrared Survey Explorer* (WISE) satellite provides all-sky photometric observations in four mid-infrared bands, $W1 = 3.4 \mu\text{m}$, $W2 = 4.6 \mu\text{m}$, $W3 = 12.0 \mu\text{m}$, $W4 = 22.8 \mu\text{m}$ (Wright et al. 2010).

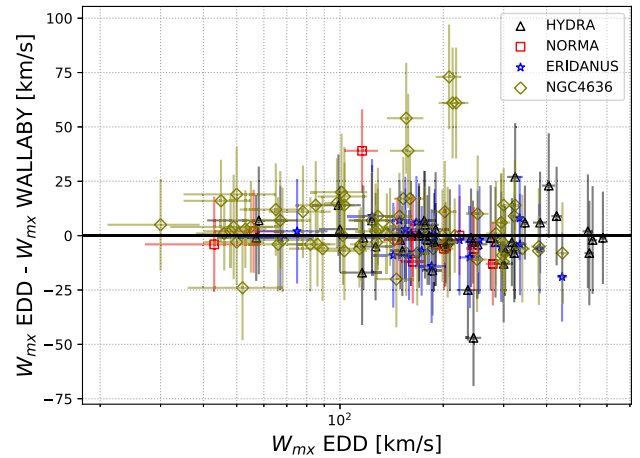


Figure 3. Comparison of the WALLABY pilot phase velocity widths presented in this article with single-dish data in the Extragalactic Distance Database (Courtois & Tully 2015). Widths are only compared where the internal error for W_{m50} in both datasets is less or equal to 20 km s^{-1} . Measurements mostly agree within the 20 km s^{-1} limit. The large offsets are either due to low-SNR Arecibo spectra, or due to noisy WALLABY spectra with residual baseline ripples due to residuals caused by strong radio continuum sources. The latter is more prominent in the NGC4636 field, which lies close to 3C273.

We initially tried to use data from the *WISE* all sky catalogue GATOR web interface. When plotting the TFR, we found that this instrumental profile-fit magnitudes were not appropriate for photometry of extended sources. As can be seen in Fig. 4, the derived TFR was totally unprobable.

Thus for this analysis, the photometric parameters are measured from the *WISE* observations using the photometric pipeline from Jarrett et al. (2013), where mosaics of each source are optimally constructed for resolved sources, carefully preserving the native angular resolution of *WISE* single frames (Jarrett et al. 2012). Source characterization includes size, shape, orientation, surface brightness, and photometric measurements.

These measurements serve as the basis for derived physical parameters, including size, luminosity, stellar mass, and star formation rate. The aggregate stellar mass is estimated using the $W1$ in-band luminosity and the $W1$ – $W2$ colour (to account for the population-dependent mass-to-light ratio), as described in Cluver et al. (2014). The global star formation rate is estimated from the $W3$ and $W4$

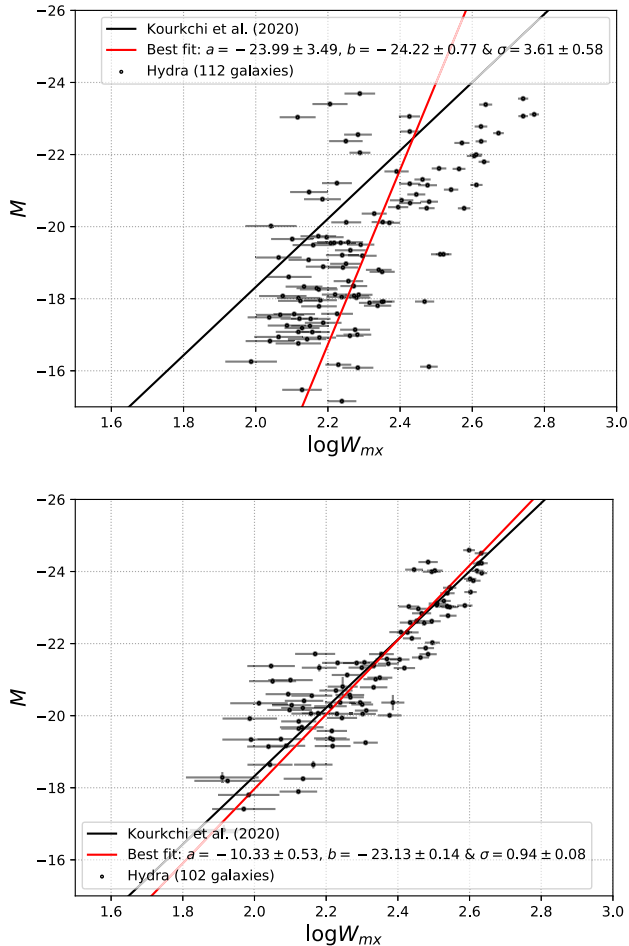


Figure 4. Comparison of TFR for Hydra using the public *WISE* photometry (top-panel) and using our newly derived *WISE* photometry. The rms deviations from the best fit line (red-line) decreases from 3.6 to 0.9 when using the new photometry. Furthermore, the best-fitting parameters are very close to the universal calibrated relation. The best-fitting parameters (red lines) are from the hyperfit package (Robotham & Obreschkow 2015), which uses errors in both axes.

spectral luminosities, after subtracting the stellar continuum, as detailed in Cluver et al. (2017), Jarrett et al. (2019).

The pipeline returns several types of apparent magnitude including, 1-sigma isophotal magnitudes, asymptotic magnitudes, and total radial-profile-modelled magnitudes. The TFR is an empirical relation between maximum rotation velocity and total luminosity, i.e total stellar mass) of the galaxy. We, therefore, used the total extrapolated magnitude, which encompasses the isophotal measured magnitude plus extrapolation of the radial SB profile to three disc scale lengths for our analysis.

The second measured parameter that is needed for the TFR is the inclination which is extracted from the *WISE* observations. We used the measured axis ratio based on the *W1* 3-sigma isophote to derive the inclination. We caution that the axis ratio, and position angle are sensitive to the angular size of the galaxy due to the relatively large beam, FWHM = 6 arcsec, of the *W1* imaging. Moreover, the near-infrared is sensitive to older stellar populations, and notably the bulge population, which tends to circularize the axis ratio and hence appear more face-on with inclination.

3 TULLY-FISHER DISTANCES

Measuring distances requires a redshift independent distance indicator, which can be either a primary indicator such as the Cepheid variable stars (Fernie 1969) or a secondary indicator such as, the TFR (Tully & Fisher 1977). In this paper, we will be adopting the TFR as our workhorse to measure distances to spiral galaxies in the four WALLABY fields. As the name suggests, a secondary distance indicator such as the TFR should be calibrated first using a sample of spiral galaxies with known distances.

Kourkchi et al. (2020a, hereafter K20) re-calibrated the TFR using optical *u*, *g*, *r*, *i*, and *z* SDSS bands as well as infrared *W1* and *W2 WISE* bands. In this article, we will use their *WISE W1* calibrated relation as our standard tool in deriving the distances of galaxies in the WALLABY fields with, as plotted in Figs 4 and 5, a slope of -9.47 ± 0.14 , a zero point of -20.36 ± 0.07 and rms of 0.58. Although, the sample used to re-calibrated the TF is different from our WALLABY sample, parameters, methods, and corrections should be as consistent as possible. In this section, we will go through all parameters that we used to derive the distances for all four WALLABY fields and their associated corrections.

With the calibrated TFR in *WISE W1* (K20) in hand, two sets of observations are required to derive TF distances: (A) spectroscopic observations (in our case HI 21-cm) from which we extract the galaxy rotational velocity; (B) photometric observations (in our case infrared imaging) from which we extract the apparent magnitude for each galaxy in our sample.

The first set of data is the WALLABY 21-cm spectra. The raw spectra were fitted using three different algorithms. The full presentation of this data set is in Section 2. To be consistent with the calibrated TFR from K20, we used the same method and corrections as CF to derive the W_{mx} line width (i.e. see Section 2.2). The only difference is that, while CF visually measured inclinations, here we are using *WISE W1* band photometric parameters (Section 2.4) to derive the inclination as:

$$\cos^2 i = \frac{(b/a)^2 - q_0^2}{1 - q_0^2}, \quad (5)$$

where q_0 is the intrinsic axial ratio of the galaxy, $q_0 = 0.13$ for Sbc, and Sc, and $q_0 = 0.2$ for other types (Giovanelli et al. 1997). We didn't make a search for the morphological type, so we used $q_0 = 0.2$, if $b/a > 0.2$ and $q_0 = 0.13$ if $b/a \leq 0.2$. Galaxies with axial ratio (b/a) greater or equal to 0.7 are excluded to avoid large corrections in the line width due to the inclination correction.

The heliocentric redshift can be measured from the WALLABY 21-cm spectra. We use redshifts to visualize the data (e.g. Figs 5 and 8). For the purpose of this paper, we first convert the heliocentric redshift z_{helio} to the CMB redshift z_{CMB} using,

$$z_{\text{CMB}} = \frac{1 + z_{\text{helio}}}{1 + z_{\text{Sun}}} - 1, \quad (6)$$

where z_{Sun} is the velocity of the sun with respect to the CMB in the direction of the galaxy being measured. It is calculated using the Planck dipole (Planck Collaboration I 2020). We derive the comoving distance $D(z_{\text{CMB}})$ in Mpc at redshift z_{CMB} , using a flat Λ CDM with $H_0 = 75 \text{ km s}^{-1} \text{ Mpc}^{-1}$ and $\Omega_m = 0.27$, and convert this to luminosity distances using:

$$D_L = (1 + z_{\text{helio}})D(z_{\text{CMB}}). \quad (7)$$

The second set of data consists of photometric imaging from *WISE W1*. The full description of the data reduction process, from building mosaics to deriving the photometric parameters of interest, is given in Section 2.4. The correction to apparent magnitudes is applied in

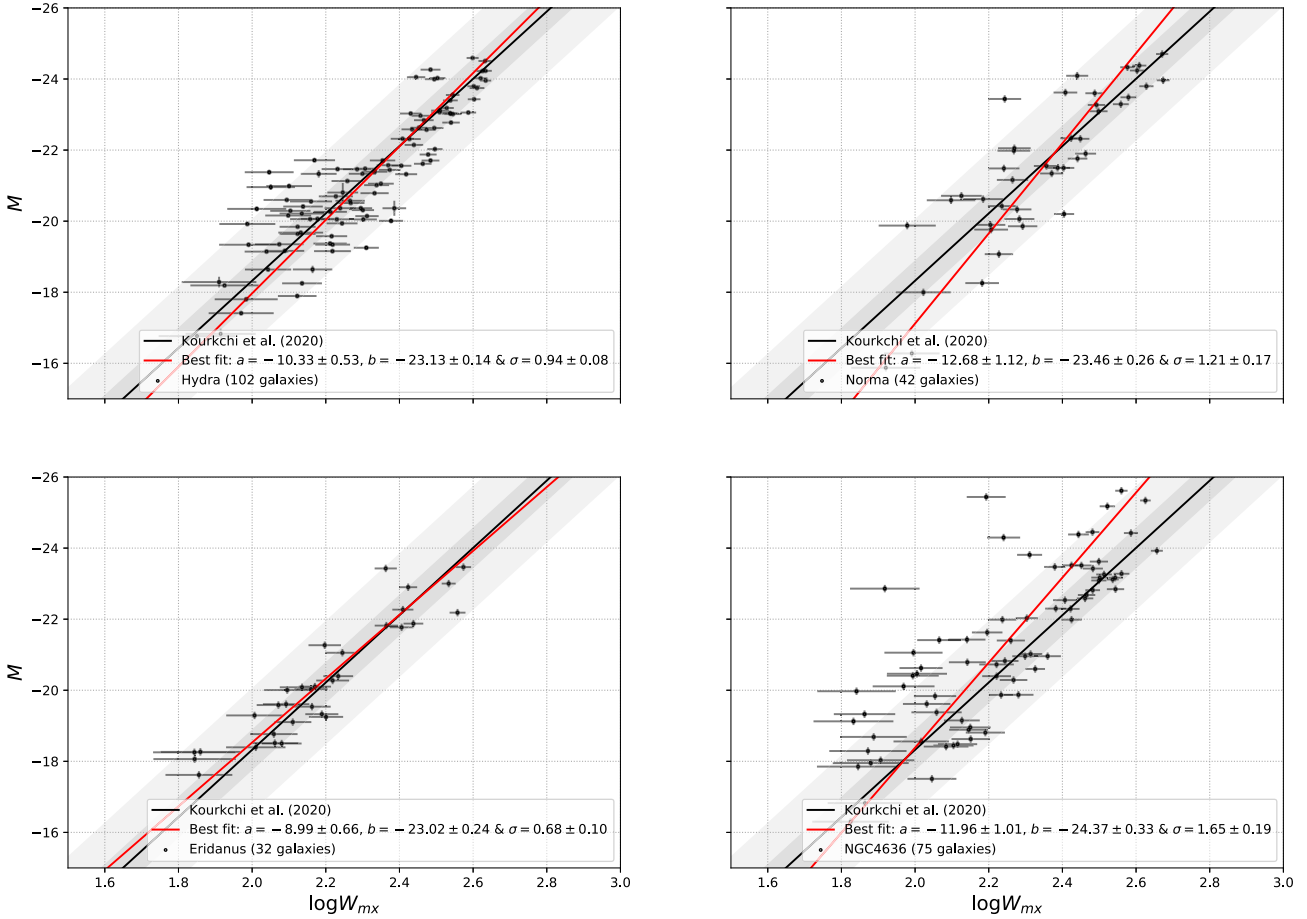


Figure 5. TFR for the four fields in the *WISE* W1 band. The solid black line is the calibrated TFR from Kourkchi et al. (2020a); the dark and light shaded areas correspond to 1- σ and 3- σ scatter around the TFR, respectively; the solid red line is the best-fitting model. The quantities derived with the Pilot survey are in good agreement with the *WISE* W1 TFR calibration in K20 in the Hydra, Norma, and Eridanus fields. The high scatter in the NGC4636 field is due to the noisy spectra caused by residual radio continuum.

the same manner as for the calibrated relation (K20):

$$m_{\text{cor}} = m_{\text{obs}} - A_{W1} - k_{W1} - I_{W1}, \quad (8)$$

where m_{cor} is the desired corrected magnitude, m_{obs} is the observed total magnitude, A_{W1} is the extinction correction due to dust from our own Galaxy (Schlegel, Finkbeiner & Davis 1998), k_{W1} is the k -correction of the form $A_{W1}^k = -2.27z$ (Oke & Sandage 1968; Huang et al. 2007), and I_{W1} is the correction for internal extinction, which were considered but neglected because they are small in W1 band. Sakai et al. (2000) parametrize them as $\gamma \log a/b$. If the effective wavelength of W1 is 3.4 μm , and the absorption in magnitudes is proportional to λ^{-1} , the maximum value is less than 0.1 mag for $\log W = 2.5$.

The absolute magnitude for each galaxy, for the purpose of visualizing the data only, was calculated as:

$$M = m_{\text{cor}} - 5 \log_{10}(D_L) - 25. \quad (9)$$

Fig. 5 visualizes the three ingredients needed for the TFR: (A) the solid line denotes the calibrated TFR in *WISE* W1 and the associated 1- σ and 3- σ regions (shaded areas); (B) the velocity width $\log W_{\text{mx}}$, on the x -axis is the maximum rotational velocity derived from the WALLABY spectra (Section 2.2); (C) the absolute magnitude M on the y -axis is derived from equation (9). The TFR fit is performed using the hyperfit method (Robotham & Obreschkow 2015), allowing varying uncertainties in both axes.

We calculated the scatter about the TFR for the four WALLABY fields in Fig. 5. The rms for Hydra is 0.90 ± 0.08 mag, which is comparable to the value of 0.89 found by K20 for the same cluster. The rms scatter in the Norma field is 1.18 ± 0.17 mag, which is slightly higher than most of the individual clusters in K20. The higher rms scatter in the TFR in Norma field is due to the strong dust extinction and stellar confusion, which affects the photometric data reduction. The scatter about the TFR in Eridanus field is 0.58 ± 0.08 mag, which is the smallest of all the four fields, and is identical to the rms scatter of the final calibrated TFR from K20. The rms scatter about the TFR in the NGC4636 region is the highest at 1.61 ± 0.19 mag. The source of this scatter may be the noisy WALLABY spectra with baseline ripples due to residuals caused by strong radio continuum sources in the NGC4636 field (see Fig. 3).

Furthermore, source finding in the NGC4636 group was done in a different way from the other fields (Hydra, Norma, and Eridanus). It was done by searching at the coordinates (RA, Dec, z) of previously catalogued galaxies, while the source finding for the other clusters was done blindly. The master catalogue providing input coordinates for NGC4636 was a combination of SDSS, ALFALFA, HIPASS, and 6dFGS. Moreover, the northern tile of the NGC4636 field consists of only a single footprint, as the other footprint had to be discarded due to data quality issues. Hence, the noise level in the northern half of the field is significantly higher than in all other fields.

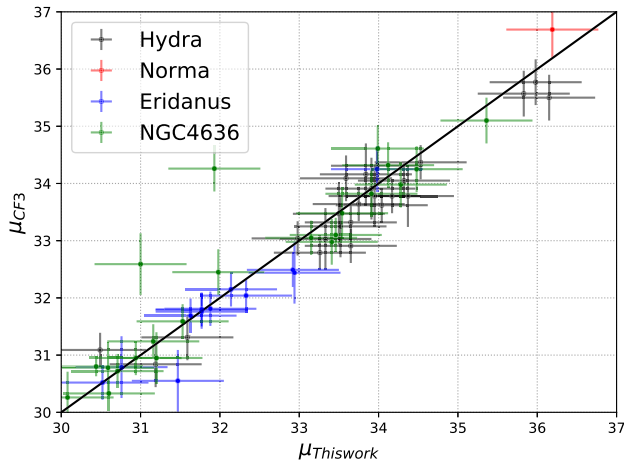


Figure 6. Comparison of the distance modulus measurements from the WALLABY pre-pilot survey (this work) versus CosmicFlows-3 (Tully et al. 2016).

With all parameters in hand, the absolute magnitude of each galaxy is calculated in this article, using the slope and zero point provided in K20 given its maximum rotational velocity :

$$M(W_{\text{mx}}) = -(20.36 \pm 0.07) - (9.47 \pm 0.14)(\log_{10} W_{\text{mx}} - 2.5) - 2.699, \quad (10)$$

where the TFR slope is (-9.47 ± 0.14) , the zero point is (-20.36 ± 0.07) , and the conversion of the AB to the Vega system is 2.699.

Using the apparent and absolute magnitude derived from equations (8) and (10), we can calculate the distance modulus as:

$$\mu = m_{\text{cor}} - M(W_{\text{mx}}). \quad (11)$$

Cross-matching with the CosmicFlows-3 (CF3) catalogue (Tully et al. 2016) result in 24 source matches in Hydra, 1 in Norma, 13 in Eridanus, and 24 in the NGC4636 field. We compared our measurements for the distance modulus to the published ones from CF3. Fig. 6 shows the comparison of the distance modulus from the four WALLABY fields with the ones from CF3. Fig. 6 shows that our measurements appear to be systematically higher than the CF3 distance moduli measurements. This can be due to the value of the zero point calibration, which was adjusted for the CF3 measurements specifically, but not for our WALLABY measurements. The zero point calibration will not be an issue for WALLABY measurements in the future, given the large sky-area, which will allow it to easily be adjusted using more accurate measurements such as SN Ia.

The distribution of the measured TF distances in the four WALLABY fields are shown in Fig. 7. The WALLABY Hydra field includes background galaxies that do not belong to the Hydra cluster. The same applies to the Norma and Eridanus fields. Measuring distances to the Hydra, Norma, NGC4636, and Eridanus clusters will, therefore, require restrictions on redshift.

Fortunately, there is a clear distinction in the redshift distribution between the galaxies in the cluster and the background galaxies in the Hydra, Norma, and Eridanus fields. Fig. 8 shows the redshift distribution in the four WALLABY fields. The dashed-red lines represent the distinction line between the cluster galaxies and the background ones. Using only galaxies with redshifts in the low-redshift side of the dashed-red lines, we measured the weighted average distance to Hydra, Norma, NGC4636, and Eridanus to be

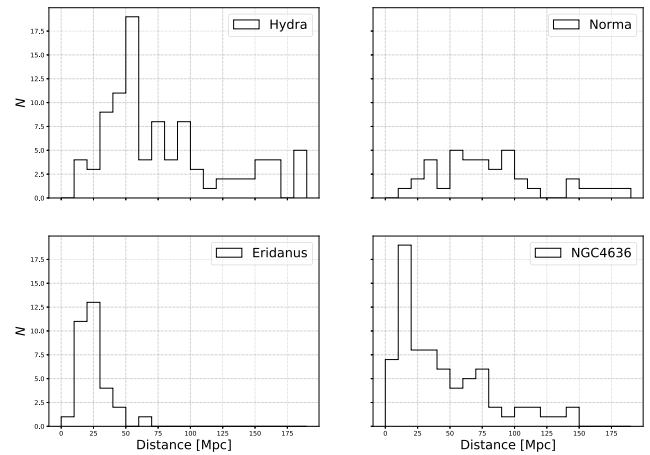


Figure 7. TFR distance distribution of galaxies in the four fields after extinction and k -corrections and the b/a cut < 0.7 using K20 calibration.

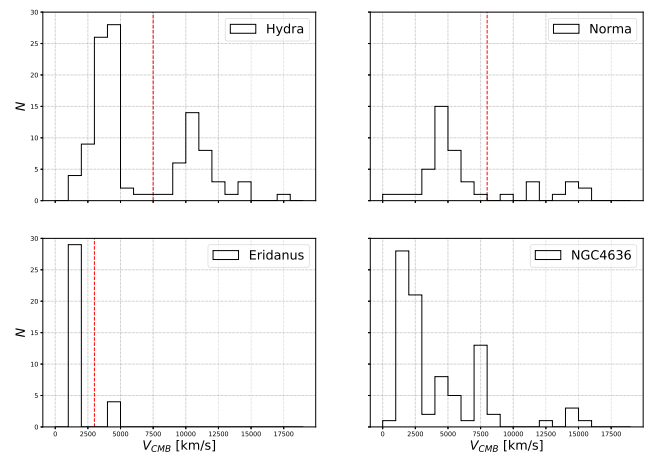


Figure 8. The redshift distribution (CMB frame) of all 614 galaxies in the Hydra, Norma, Eridanus, and NGC4636 fields. The dashed-red lines in the Hydra, Norma, and Eridanus plots represent the estimated division between the cluster and background galaxies. The WALLABY pilot integration time allows the detection of galaxies located at 15 000 km s⁻¹, around twice the distance limit of previous single dish surveys such as HIPASS.

53.5 ± 2.5 , 69.4 ± 5.5 , 23.0 ± 2.1 , and 21.5 ± 1.4 Mpc, respectively. In this study, the Norma distance refers to the eastern overdensity (which is part of the Norma supercluster). This distance may be slightly different from the cluster distance due to filament projection. In the next section, a comparison with previous determinations of these distances will be made.

Peculiar velocities are the non-Hubble velocities induced gravitationally by large-scale structure. For a Hubble Constant between 68 and 73 km s⁻¹ Mpc⁻¹, the peculiar velocities with respect to the CMB of the Hydra, Norma, NGC4636, and Eridanus clusters lie in the range $(-320, -40)$, $(-730, -350)$, $(300, 430)$, and $(0, 110)$ km s⁻¹, respectively.

4 SPATIAL DISTRIBUTION OF GALAXIES IN THE PHASE 1 PILOT SURVEY

Fig. 8 illustrates the variance in the redshift distribution between the WALLABY pilot survey fields, and the presence of cluster foreground and background galaxies. It also shows that the pilot integration times allow us to reach a recessional velocity of

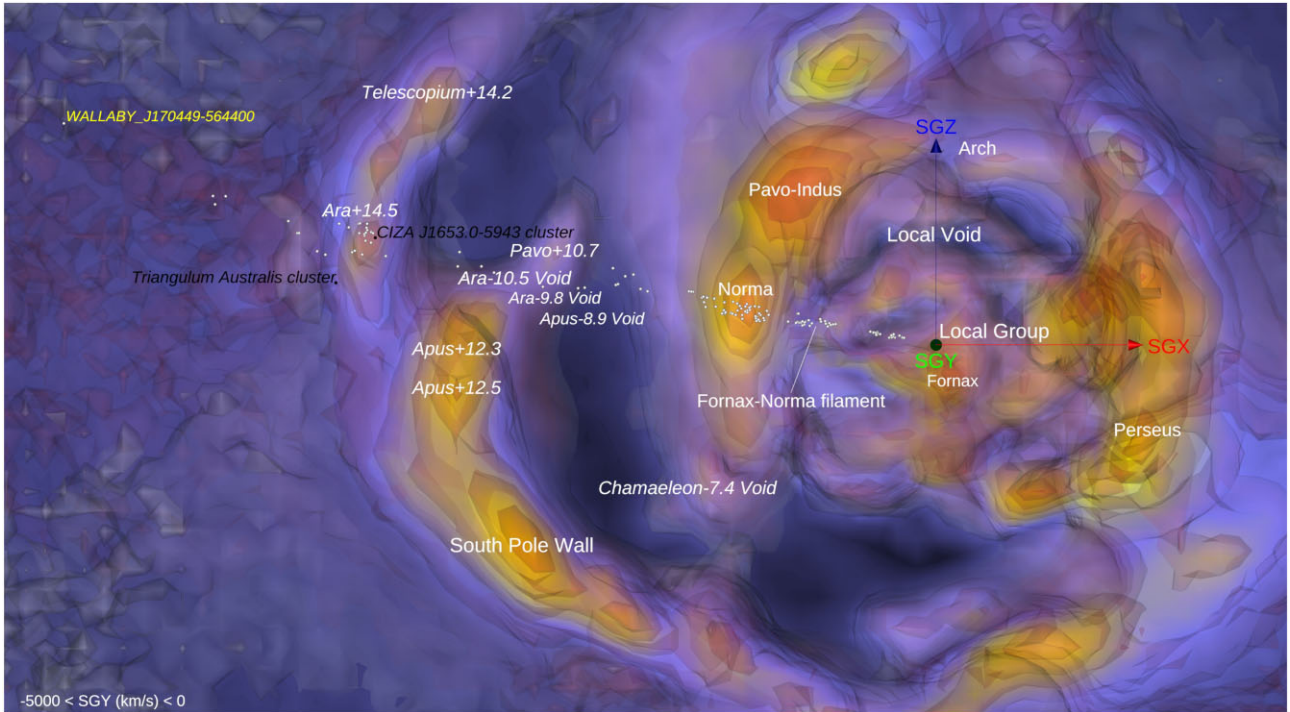


Figure 9. Map of the redshift positions of galaxies in the Norma field (white points) overlaid on the (coloured) density contrast field (δ) as reconstructed from the CosmicFlows-3 Catalog of peculiar velocities. Scale and orientation are provided by the red and blue 5000 km s⁻¹-long arrows, emanating from our position and associated with the supergalactic coordinates SGX and SGY, respectively. A slice defined by $0 > \text{SGY} > -5000$ km s⁻¹ is, here, seen from the negative SGY direction. This static view is complemented by an [online interactive 3D visualization](#) of the Norma survey field showing three levels of the overdensity δ , field. This tool can be used to better grasp how the field includes a series of voids and overdensities.

15 000 km s⁻¹, doubling what has been achieved by predecessor all-sky surveys reliant on single dish observations, such as 2MTF. These higher redshifts have so far only been accessible using fundamental plane techniques – e.g. 6dFGS, which provides about 6000 useful peculiar velocities. WALLABY is expected to deliver about 30 000–50 000 peculiar velocities.

4.1 Hydra and Norma cluster fields

The Hydra cluster has a mean redshift of 0.012 (Babyk & Vavilova 2013) and a velocity dispersion of 690 km s⁻¹ (Lima-Dias et al. 2021). Fig. 8 shows the redshift distribution for Hydra cluster galaxies in our sample whereas Fig. 5 shows the TFR for these galaxies.

Woudt et al. (2008) find a mean velocity of 4871 ± 54 km s⁻¹ for the Norma cluster and locate its centre at $(l, b) = (325.3^\circ, -7.2^\circ)$. They identify it as the richest cluster in the region of the Great Attractor. Mutabazi (2021), in a study of its fundamental plane, finds a small peculiar velocity. The WALLABY pilot survey field is centred on $(l, b) = (329.3^\circ, -10.4^\circ)$, i.e. 5.1° , respectively, 6 Mpc from the cluster centre. Nevertheless, there is clear overdensity of galaxies visible at the cluster redshift (Fig. 8).

A full 3D view of the Great Attractor region with the first CF reconstruction of the local velocity field near Norma and Hydra clusters was presented by Courtois et al. (2012). Infall to the Norma cluster takes the form of a sharper distribution in redshift space than in real space (see Fig. 9).

The positions of WALLABY galaxies within the Cosmic Web can be studied using the full matter (dark and luminous) density

contrast field (usually noted δ) reconstructed from the CosmicFlows-3 Catalog of peculiar velocities (Courtois et al. 2019; Graziani et al. 2019; Tully et al. 2019; Pomarède et al. 2020). Fig. 9 shows the redshift locations of galaxies of the Norma survey versus a real-space three-dimensional visualization of the overdensity field, restricted to a slice. The visualization is obtained by a combination of a ray-casting algorithm (Pomarède et al. 2017a) resulting in a smooth rendering of the δ overdensity field ranging from most underdense (deep blue colour) to most overdense (yellow), and a series of semitransparent isosurface polygons resulting in a sharp materialization of the surfaces ranging from $\delta = 0$ (grey surface) to highly overdense ($\delta = 2.8$ in red). The grey surface, hence, marks the frontier between the underdense and the overdense Universe. The most noticeable feature in the distribution of WALLABY galaxies is their aggregation near the Norma cluster at $\text{SGX} \simeq -5000$ km s⁻¹, seen as a pronounced local maximum in the density contrast field (δ field). Between the Local Group and the Norma cluster, the field includes a section of the Local Void (Tully et al. 2019), and the termination of a filament connecting the Fornax cluster to the Norma cluster, as can better be seen from the interactive 3D visualization supplementing Fig. 9 (see annotations 2 and 3). Beyond the Norma–Pavo–Indus filament (Fairall 1998; Courtois et al. 2013), the field includes the void separating this filament and the South Pole Wall (Pomarède et al. 2020). The map of Fig. 9 indicates the location of local extrema of the over and underdensity field δ , such as the Ara-10.5 Void and the Ara+14.5 overdensity, whose names include the name of the constellation in which they sit, followed by a ‘+’ for an overdensity or a ‘-’ for an underdensity, followed by their redshift in units of 1000 km s⁻¹, a convention established in Tully et al. (2019).

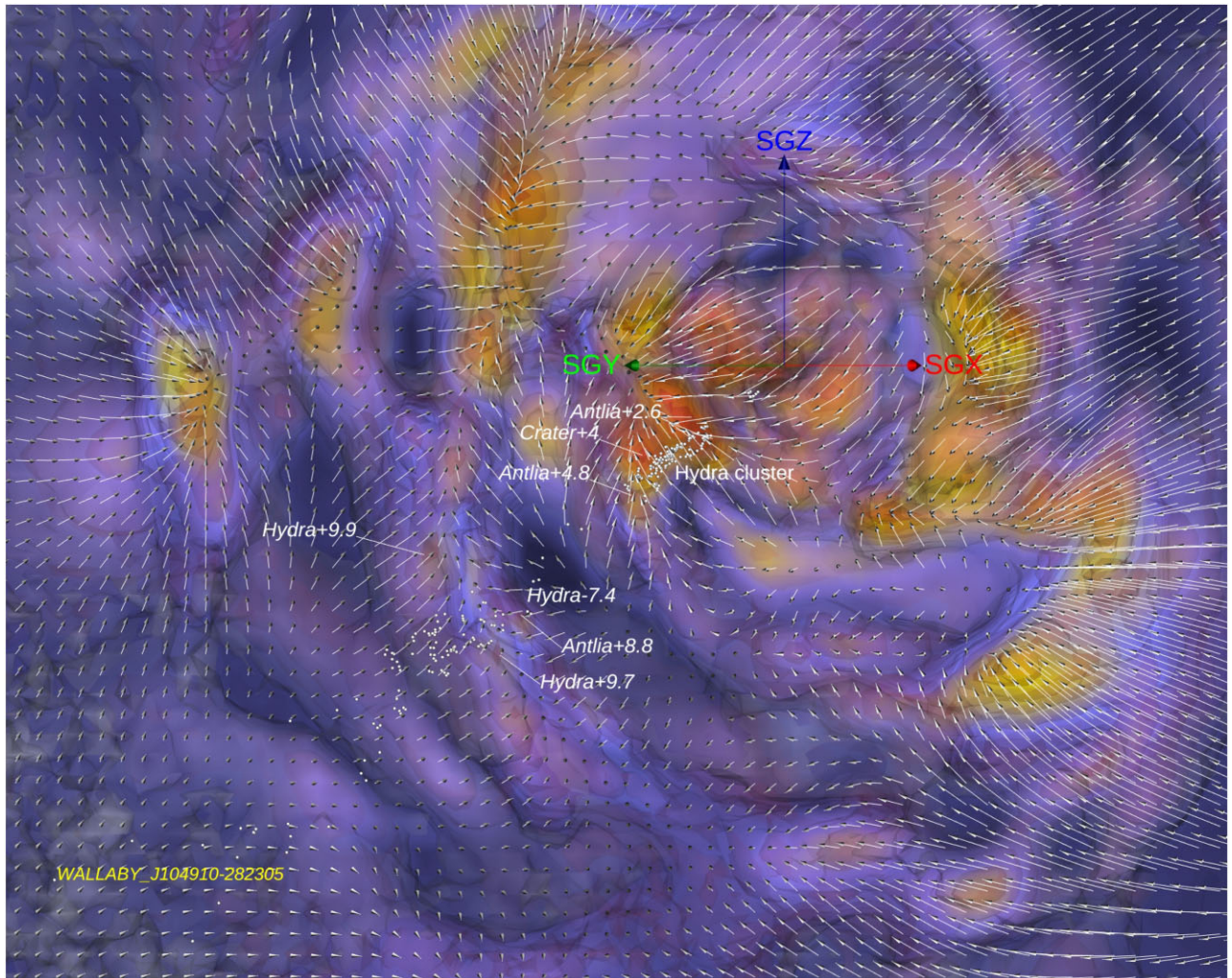


Figure 10. Map of the redshift positions of galaxies in the Hydra field (white points) overlaid on the (coloured) full matter (dark + luminous) density contrast δ , field, and the peculiar (gravitational) velocity field (white arrows) as reconstructed from the CosmicFlows-3 Catalogue. Scale and orientation are provided by the red, green, and blue 5000 km s^{-1} -long arrows emanating from our position and associated with the three cardinal axes of the supergalactic coordinate system SGX, SGY, and SGZ, respectively. A slice of 5000 km s^{-1} -thickness centred on the plane defined by the supergalactic longitude of the Hydra cluster ($\text{SGL} = 139.36^\circ$) is here seen face-on. This static view is complemented by an [online interactive 3D visualization](#) of the Hydra survey beam showing three levels of the overdensity δ , field. This tool can be used to better grasp how the field includes a series of voids and overdensities.

An aggregation of WALLABY galaxies is found at the location of the Ara+14.5 knot of the Cosmic Web, that is nearly coincident with the CIZA J1653.0-5943 cluster (Ebeling, Mullis & Tully 2002). Beyond this, most distant section of the South Pole Wall, the field presumably enters a new void, in regions where the CosmicFlows-3 reconstruction tends to a null field due lack of sufficient data. The most distant galaxy in the Norma field, located at redshift 0.073, is indicated on the map.

In Fig. 10, the distribution of the WALLABY galaxies in the Hydra field is plotted in a similar way on top of the CosmicFlows-3 cosmography. The density of WALLABY galaxies as a function of distance displays contrasting features: after displaying a handful of galaxies located in our vicinity at $\simeq 900 \text{ km s}^{-1}$, no galaxies are detected in the void located in the foreground of the Hydra cluster. A major aggregation of objects is then seen at the crossing of the Hydra cluster, which is part of a high-density node in the Cosmic Web, as seen in the map of the CosmicFlows-3 density contrast. In the

background of the Hydra cluster, the surveyed region includes a deep void (Hydra-7.4), where very few galaxies reside. In the background of this void, there is an extended cloud of galaxies scattered throughout a wall located in Hydra at about $10\,000 \text{ km s}^{-1}$, where local maxima in the density are found: Hydra+9.7, Hydra+9.9, and Antlia+8.8. After dropping as a function of distance, the number density of galaxy rises again at the most extreme distances, with WALLABY J104910-282305 being the most remote one at $\sim 23\,000 \text{ km s}^{-1}$. This infall pattern of peculiar velocities leads to a higher overdensity in redshift space (Fig. 8) than in real space (Fig. 7).

4.2 The NGC4636 cluster and Eridanus fields

The spatial distribution of the galaxies of the NGC4636 survey is shown in Fig. 11. The highest density in the field is at the crossing of the Virgo Strand (Courtois et al. 2013), a section of the

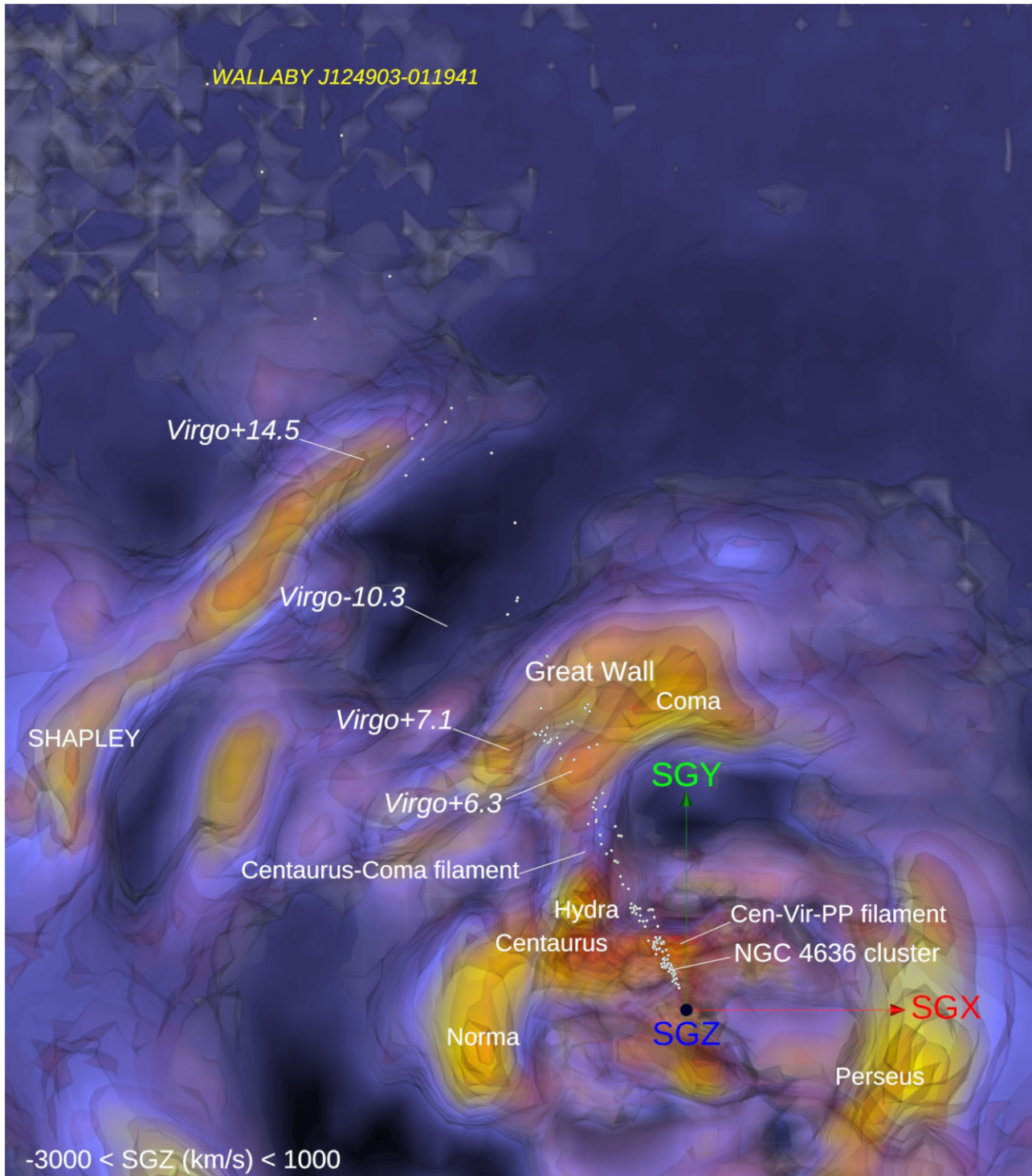


Figure 11. Map of the redshift positions of galaxies in the NGC4636 field (white points) overlaid on the (coloured) density contrast δ , as reconstructed from the CosmicFlows-3 Catalog of peculiar velocities. Scale and orientation are provided by the red and green 5000 km s^{-1} -long arrows emanating from our position and associated with supergalactic coordinates SGX and SGY, respectively. A slice contained defined by $1000 > \text{SGZ} > -3000 \text{ km s}^{-1}$ is here seen from the positive SGZ direction. This static view is complemented by an [online interactive 3D visualization](#) of the NGC4636 survey field.

Cen-Vir-PP filament that connects the Centaurus and Perseus nodes of the Cosmic Web through the Virgo cluster (Pomarède et al. 2017b), in which the NGC4636 cluster is nested. Beyond the cluster, the field includes the outskirts of the void located between Virgo and the Great

Wall (Gregory & Thompson 1978), and also includes part of the Centaurus-Coma filament (Pomarède et al. 2017b). The number of galaxies then rises at the intersection of the Great Wall (de Lapparent, Geller & Huchra 1986) near the Virgo+6.3 and Virgo+7.1 local

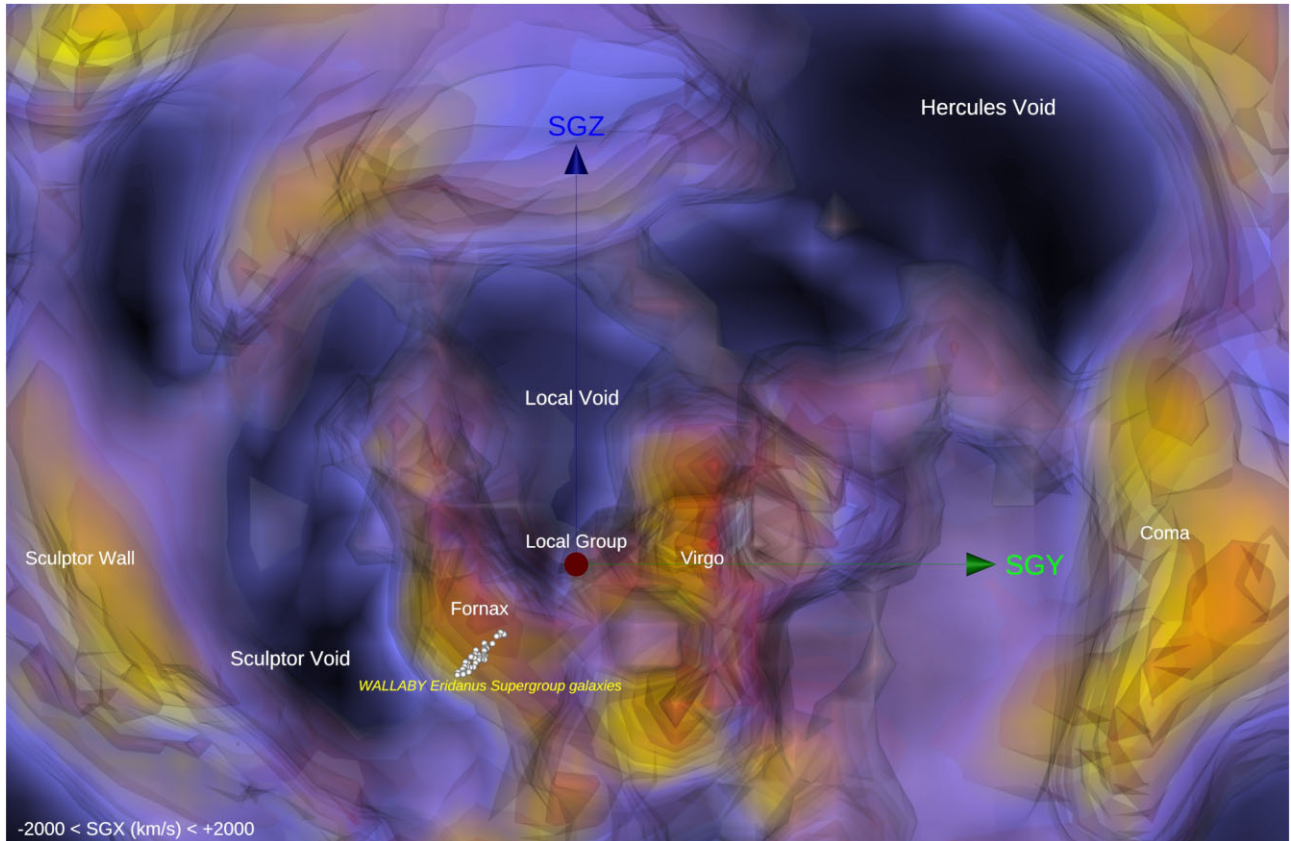


Figure 12. Map of the redshift positions of galaxies in the Eridanus super group (white points) overlaid on the (coloured) density contrast δ , as reconstructed from the CosmicFlows-3 Catalog of peculiar velocities. Scale and orientation are provided by green and blue 5000 km s^{-1} -long arrows emanating from our position and associated with supergalactic coordinates SGY and SGZ, respectively. A slice defined by $2000 > \text{SGX} > -2000 \text{ km s}^{-1}$ is here seen from the positive SGX direction. This static view is complemented by an [online interactive 3D visualization](#) of the Eridanus super group survey.

maxima of the density contrast. In the background of the Great Wall, there is the trough and peak of Virgo-10.3 and Virgo+14.5.

Finally, the location of the galaxies of the Eridanus super group survey is presented in Fig. 12. It shows that the galaxies are found near the Fornax node in the Cosmic Web, and distributed along the density gradient seen in the transition toward the Sculptor Void located in the background (Pellegrini et al. 1990; Fairall 1998).

4.3 Discussion

The cosmographic maps presented in the previous section demonstrate that the WALLABY pilot survey fields probe a vast diversity of elements of the cosmic web: intersecting numerous features such as voids, filaments, walls, and the nodes which host the targeted clusters. The future inclusion of WALLABY-detected galaxies in the CosmicFlows collection will add useful data for cosmographical purposes. Of particular interest are the regions around the Hydra and Norma clusters, and their roles in the dynamical structure and influence of the Great Attractor (Dressler et al. 1987; Woudt et al. 2008; Tully et al. 2014; Hoffman et al. 2017). WALLABY has the advantage of being able to peer through the Galactic Plane, permitting the study of the so-called Zone of Avoidance, which limits optical/IR surveys. Also of great interest are galaxies that reside in voids, which will provide improved constraints on the flows evacuating these underdense patches (Tully et al. 2008; Rizzi et al. 2017; Shaya et al. 2017). The most distant sections of the

pilot fields, with velocities out to $22\,000 \text{ km s}^{-1}$, will bring in new useful information on the architecture of the Cosmic Web in remote locations, thus providing better measurements of the large-scale gravitational field than currently available, and potentially providing a definitive explanation for the amplitude of the CMB dipole.

In the vicinity of the Great Attractor, peculiar velocities for the Hydra and Norma fields show an infall pattern towards the respective clusters, i.e. positive peculiar velocities on the nearside of the clusters and negative on the far side. Beyond Hydra, positive velocities return as the galaxies come under the influence of the wall located at about $10\,000 \text{ km s}^{-1} \simeq 135 \text{ Mpc}$, seen in Fig. 10 at the locations of the local maxima Hydra+9.7 and Hydra+9.9. The pattern observed in the peculiar velocities at $\sim 100 \text{ Mpc}$ is typical of an evacuation by the void located at 7400 km s^{-1} , labelled Hydra-7.4 in Fig. 10, where galaxies located in the foreground of this void have negative velocities, while galaxies located in the background have positive velocities. The wealth of data represented by the WALLABY galaxies located in this direction at large distance will play an important role in mapping the structure currently hinted at by the CosmicFlows-3 reconstruction, in particular of the wall seen in Hydra at $10\,000 \text{ km s}^{-1}$.

5 CONCLUSIONS

The Tully–Fisher distance of the Eridanus group is $21.5 \pm 1.4 \text{ Mpc}$, and its peculiar velocity for a Hubble constant of $68\text{--}73 \text{ km s}^{-1} \text{ Mpc}^{-1}$ is small, between 0 and 110 km s^{-1} . The NGC4636

group is a complex structure within the Virgo cluster zero velocity surface, and its Tully–Fisher distance is 23.0 ± 2.1 Mpc. Under the same assumptions, its peculiar velocity is $300\text{--}430$ km s⁻¹. The distance of the Hydra cluster is 53.5 ± 2.5 Mpc. There is a substantial background group associated with the Shapley Supercluster. We measure a peculiar velocity of -320 to -40 km s⁻¹ for the Hydra cluster, assuming $68 < H_0 < 73$ km s⁻¹ Mpc⁻¹. The Norma cluster is the most distant in the present sample at 69.4 ± 5.5 Mpc. Its peculiar velocity is -350 to -730 km s⁻¹ under the same assumptions.

This study also aims at testing the reliability, accuracy, and dynamic range in distance able to be provided by Tully–Fisher distances for galaxies detected and parametrized in the pre-pilot and Phase 1 surveys of WALLABY. It is also a prediction for what the full survey will deliver. We find that :

(i) Measurements of galaxy velocity widths are in excellent agreement with those measured using previous single-dish observations with typical discrepancies around 7 km s⁻¹, validating both the data quality and observational strategy of WALLABY. The WALLABY Tully–Fisher distances have uncertainties at the level of 5 to 10 percent, which are similar or better than the accuracy obtained with single dish observations.

(ii) Even as close to the Zone of Avoidance as the Norma cluster, H I spectra provided by the SoFiA pipeline are excellent and extinction in the *WISE* W1 band is less than 0.1 mag. The combination of WALLABY and *WISE* W1 band observations will enable investigation of large number of accurate peculiar velocities of galaxies in the upcoming full WALLABY survey. The Tully–Fisher dispersion obtained is at the level of 0.9 unit, which is excellent for these cluster fields.

(iii) The distribution of galaxies and kinematic pattern in the Hydra and Norma fields is one of infall to the cluster mass concentrations.

(iv) The WALLABY pilot survey sensitivity and widefield capability will extend the investigation of peculiar velocities beyond what was previously achieved with the single dish TFR method. WALLABY will detect about 500 k galaxies at a mean redshift of $z = 0.05$. If 251 out of 614 of the pilot phase 1 galaxies pass the S/N and inclination tests, this might suggest that 200 k Tully–Fisher distances would result from WALLABY – much higher than was expected in initial proposals and increasing by a factor of twenty the current number of Tully–Fisher distances in Cosmic-Flows-4. The number may be slightly optimistic given that we only observed nearby structures on Phase 1. However, most fields should have their peak redshift at 0.04, well beyond these local structures.

ACKNOWLEDGEMENTS

The Australian SKA Pathfinder is part of the Australia Telescope National Facility, which is managed by CSIRO. Operation of ASKAP is funded by the Australian Government with support from the National Collaborative Research Infrastructure Strategy. ASKAP uses the resources of the Pawsey Supercomputing Centre. Establishment of ASKAP, the Murchison Radio-astronomy Observatory, and the Pawsey Supercomputing Centre are initiatives of the Australian Government, with support from the Government of Western Australia and the Science and Industry Endowment Fund. We acknowledge the Wajarri Yamatji people as the traditional owners of the Observatory site. Parts of this research were supported by the Australian Research Council Centre of Excellence for All Sky Astrophysics in 3 Dimensions (ASTRO 3D), through project number CE170100013. We would like to thank all our colleagues on the WALLABY team

for helpful discussions. We have made use of NASA data products, including *WISE* and NED, and also NSF OIR Lab data products. We acknowledge the use of the HyperLeda data base. HC is grateful to the Institut Universitaire de France and CNES for its support. KS, CH, and TD are supported by the Australian Government through the Australian Research Council’s Laureate Fellowship funding scheme (project FL180100168). AD acknowledges financial support from the Project IDEXLYON at the University of Lyon under the Investments for the Future Program (ANR-16-IDEX-0005). AB acknowledges support from the Centre National d’Etudes Spatiales (CNES), France. DK acknowledges funding from the European Research Council (ERC), under the European Union’s Horizon 2020 research and innovation programme (grant agreement no. 679627; project name FORNAX). RCKK is supported by the South African Research Chairs Initiative of the Department of Science and Technology and National Research Foundation. FB acknowledges funding from the European Research Council (ERC) under the European Union’s Horizon 2020 research and innovation programme (grant agreement No.726384/Empire). AD is supported by a KIAS Individual Grant (PG087201) at Korea Institute for Advanced Study. Many thanks to Dmitry Makarov for helping us on the cross-identification with galaxy PGC names.

REFERENCES

- Aaronson M., Huchra J., Mould J., 1979, *ApJ*, 229, 1
 Babyk I. V., Vavilova I. B., 2013, *OAP*, 26, 175
 Cluver M. E. et al., 2014, *ApJ*, 782, 90
 Cluver M. E., Jarrett T. H., Dale D. A., Smith J. D. T., August T., Brown M. J. I., 2017, *ApJ*, 850, 68
 Courtois H. M., Tully R. B., 2015, *MNRAS*, 447, 1531
 Courtois H. M., Tully R. B., Fisher J. R., Bonhomme N., Zavodny M., Barnes A., 2009, *AJ*, 138, 1938
 Courtois H. M., Tully R. B., Makarov D. I., Mitronova S., Koribalski B., Karachentsev I. D., Fisher J. R., 2011a, *MNRAS*, 414, 2005
 Courtois H. M., Tully R. B., Héraudeau P., 2011b, *MNRAS*, 415, 1935
 Courtois H. M., Hoffman Y., Tully R. B., Gottlöber S., 2012, *ApJ*, 744, 43
 Courtois H. M., Pomarède D., Tully R. B., Hoffman Y., Courtois D., 2013, *AJ*, 146, 69
 Courtois H. M., Kraan-Korteweg R. C., Dupuy A., Graziani R., Libeskind N. I., 2019, *MNRAS*, 490, L57
 de Lapparent V., Geller M. J., Huchra J. P., 1986, *ApJ*, 302, L1
 Dressler A., Faber S. M., Burstein D., Davies R. L., Lynden-Bell D., Terlevich R. J., Wegner G., 1987, *ApJ*, 313, L37
 Ebeling H., Mullis C. R., Tully R. B., 2002, *ApJ*, 580, 774
 Fairall A. P., 1998, *Large-Scale Structures in the Universe*. Wiley, New York
 Fernie J. D., 1969, *PASP*, 81, 707
 For B. Q. et al., 2021, *MNRAS*, 507, 2300
 Giovanelli R., Haynes M. P., Herter T., Vogt N. P., da Costa L. N., Freudling W., Salzer J. J., Wegner G., 1997, *AJ*, 113, 53
 Graziani R., Courtois H. M., Lavaux G., Hoffman Y., Tully R. B., Copin Y., Pomarède D., 2019, *MNRAS*, 488, 5438
 Gregory S. A., Thompson L. A., 1978, *ApJ*, 222, 784
 Haynes M. P. et al., 2018, *ApJ*, 861, 49
 Hoffman Y., Courtois H. M., Tully R. B., 2015, *MNRAS*, 449, 4494
 Hoffman Y., Pomarède D., Tully R. B., Courtois H. M., 2017, *Nat. Astron.*, 1, 0036
 Hong T. et al., 2019, *MNRAS*, 487, 2061
 Hotan A. W. et al., 2021, *PASA*, 38, e009
 Huang J. S. et al., 2007, *ApJ*, 664, 840
 Jarrett T. H. et al., 2012, *AJ*, 144, 68
 Jarrett T. H. et al., 2013, *AJ*, 145, 6
 Jarrett T. H., Cluver M. E., Brown M. J. I., Dale D. A., Tsai C. W., Masci F., 2019, *ApJS*, 245, 25

- Koribalski B. S. et al., 2004, *AJ*, 128, 16
 Koribalski B. S. et al., 2020, *Ap&SS*, 365, 118
 Kourkchi E., Tully R. B., Neill J. D., Seibert M., Courtois H. M., Dupuy A., 2020a, *ApJ*, 884, 82 (K20)
 Kourkchi E. et al., 2020b, *ApJ*, 902, 145
 Lagattuta D. J., Mould J. R., Staveley-Smith L., Hong T., Springob C. M., Masters K. L., Koribalski B. S., Jones D. H., 2013, *ApJ*, 771, 88
 Lima-Dias C. et al., 2021, *MNRAS*, 500, 1323
 Meyer M. J. et al., 2004, *MNRAS*, 350, 1195
 Mould J., 2020, *Front. Astron. Space Sci.*, 7, 21
 Mutabazi T., 2021, *ApJ*, 911, 16
 Neill J. D., Seibert M., Tully R. B., Courtois H., Sorce J. G., Jarrett T. H., Scowcroft V., Masci F. J., 2014, *ApJ*, 792, 129
 Oke J. B., Sandage A., 1968, *ApJ*, 154, 21
 Pellegrini P. S., da Costa L. N., Huchra J. P., Latham D. W., Willmer C. N. A., 1990, *AJ*, 99, 751
 Peterson E. R. et al., 2022, *ApJ*, 938, 112
 Planck Collaboration I, 2020, *A&A*, 641, A1
 Pomarède D., Courtois H. M., Hoffman Y., Tully R. B., 2017a, *PASP*, 129, 058002
 Pomarède D., Hoffman Y., Courtois H. M., Tully R. B., 2017b, *ApJ*, 845, 55
 Pomarède D., Tully R. B., Graziani R., Courtois H. M., Hoffman Y., Lezmy J., 2020, *ApJ*, 897, 133
 Ponomareva A. A. et al., 2021, *MNRAS*, 508, 1195
 Rizzi L., Tully R. B., Shaya E. J., Kourkchi E., Karachentsev I. D., 2017, *ApJ*, 835, 78
 Robotham A. S. G., Obreschkow D., 2015, *PASA*, 32, e033
 Said K., Kraan-Korteweg R. C., Staveley-Smith L., Williams W. L., Jarrett T. H., Springob C. M., 2016, *MNRAS*, 457, 2366 (S16)
 Said K., Colless M., Magoulas C., Lucey J. R., Hudson M. J., 2020, *MNRAS*, 497, 1275
 Sakai S. et al., 2000, *ApJ*, 529, 698
 Schlegel D. J., Finkbeiner D. P., Davis M., 1998, *ApJ*, 500, 525
 Serra P. et al., 2015, *MNRAS*, 448, 1922
 Shaya E. J., Tully R. B., Hoffman Y., Pomarède D., 2017, *ApJ*, 850, 207
 Sorce J. G. et al., 2013, *ApJ*, 765, 94
 Springel V. et al., 2018, *MNRAS*, 475, 676
 Thévenot M., Cornen C., Goodwin B. L., Macmillan C., Stenner A. G., Téglás B., 2020, *RNAAS*, 4, 159
 Tully R. B., Fisher J. R., 1977, *A&A*, 54, 661
 Tully R. B., Fouqué P., 1985, *ApJS*, 58, 67
 Tully R. B., Shaya E. J., Karachentsev I. D., Courtois H. M., Kocevski D. D., Rizzi L., Peel A., 2008, *ApJ*, 676, 184
 Tully R. B., Courtois H., Hoffman Y., Pomarède D., 2014, *Nature*, 513, 71
 Tully R. B., Courtois H. M., Sorce J. G., 2016, *AJ*, 152, 50
 Tully R. B., Pomarède D., Graziani R., Courtois H. M., Hoffman Y., Shaya E. J., 2019, *ApJ*, 880, 24
 Wang J. et al., 2021, *ApJ*, 915, 70
 Westmeier T. et al., 2021, *MNRAS*, 506, 3962
 Westmeier T. et al., 2022, *Publ. Astron. Soc. Aust.*, 39, e058
 Wong O. I. et al., 2021, *MNRAS*, 507, 2905
 Woudt P. A., Kraan-Korteweg R. C., Lucey J., Fairall A. P., Moore S. A. W., 2008, *MNRAS*, 383, 445
 Wright E. L. et al., 2010, *AJ*, 140, 1868

APPENDIX A: DATA

Tables in Appendix A present four catalogues of Hydra, Norma, Eridanus, and NGC4636. The parameters listed in the catalogues are:

Column (1) - WALLABY ID as reported in the WALLABY Pilot Survey data release (Westmeier et al. 2022).

Columns (2) - Principal Galaxies Catalogue number (PGC)

Columns (3 and 4) - Right Ascension (RA) and Declination (Dec.) in the J2000.0 epoch of the fitted position in WALLABY.

Column (5) - *WISE* *W1* total magnitude after Galactic extinction and *k* corrections.

Column (6) - Inclination calculated from *WISE* (*b/a*) as in equation (5).

Column (7) - Linewidths corrected for inclination.

Column (8) - CMB redshifts.

Column (9) - Tully–Fisher luminosity distances in Mpc.

Column (10 and 11) - Distance modulus and associated error.

Table A1. Hydra H1 data from WALLABY phase 1 pilot survey.

| Name | PGC | RA | DEC | $W_{\text{I}}_{\text{tot}}$ | i | W_{mx} | z_{cmb} | d_{L} | μ | e_{μ} |
|----------------|---------|----------|----------|-----------------------------|---------|-----------------|------------------|----------------|-------|-----------|
| J100342-270137 | 29166 | 150.9256 | -27.0271 | 10.715 | 79.3316 | 185.2012 | 0.00430152 | 20.0 | 31.5 | 0.58 |
| J100351-273417 | 29179 | 150.9662 | -27.5715 | 8.947 | 51.0182 | 421.9486 | 0.01043229 | 42.1 | 33.12 | 0.58 |
| J100426-282638 | 29216 | 151.1091 | -28.4442 | 9.9561 | 73.1772 | 202.6735 | 0.00471975 | 16.7 | 31.12 | 0.58 |
| J100640-273917 | 29378 | 151.667 | -27.6549 | 12.923 | 62.8353 | 223.6714 | 0.01536106 | 79.0 | 34.49 | 0.58 |
| J100808-260942 | 29470 | 152.0353 | -26.1618 | 13.4138 | 57.4373 | 132.8899 | 0.01141974 | 36.9 | 32.84 | 0.58 |
| J100830-262140 | 768685 | 152.1256 | -26.3611 | 14.5217 | 76.0108 | 118.515 | 0.01512221 | 49.5 | 33.47 | 0.58 |
| J100939-290112 | 154738 | 152.4128 | -29.0202 | 12.4737 | 47.9538 | 278.7484 | 0.0480433 | 97.4 | 34.94 | 0.58 |
| J101025-275214 | 748738 | 152.6054 | -27.8708 | 13.1662 | 68.9346 | 132.8803 | 0.00919987 | 33.0 | 32.59 | 0.58 |
| J101208-252000 | 154861 | 153.0362 | -25.3335 | 12.2087 | 58.4722 | 305.026 | 0.04684504 | 102.3 | 35.05 | 0.58 |
| J101221-254604 | 29719 | 153.0904 | -25.7678 | 11.4898 | 60.6661 | 430.1545 | 0.03330433 | 140.9 | 35.74 | 0.58 |
| J101247-275028 | 29743 | 153.1998 | -27.8413 | 9.4937 | 76.0108 | 350.3921 | 0.00984753 | 38.1 | 32.9 | 0.58 |
| J101247-291053 | 732369 | 153.1962 | -29.1815 | 13.2847 | 61.97 | 267.361 | 0.03197037 | 130.8 | 35.58 | 0.58 |
| J101348-273147 | 29821 | 153.4516 | -27.5299 | 13.3432 | 57.7338 | 164.3848 | 0.00981759 | 53.5 | 33.64 | 0.58 |
| J101357-262550 | - | 153.4904 | -26.4308 | 15.1772 | 52.8182 | 102.9217 | 0.03382259 | 51.3 | 33.55 | 0.58 |
| J101359-253824 | 29836 | 153.4964 | -25.64 | 13.2213 | 71.1098 | 205.0435 | 0.01177462 | 76.9 | 34.43 | 0.58 |
| J101359-274538 | - | 153.4978 | -27.7607 | 15.9193 | 73.7025 | 70.8468 | 0.00969587 | 35.6 | 32.76 | 0.59 |
| J101438-272431 | 29888 | 153.661 | -27.4087 | 10.8963 | 54.1261 | 386.2726 | 0.01496544 | 87.4 | 34.71 | 0.58 |
| J101441-285221 | 29892 | 153.6744 | -28.8726 | 7.4814 | 71.9901 | 312.3018 | 0.00479612 | 12.1 | 30.42 | 0.58 |
| J101448-285723 | 29903 | 153.7006 | -28.9565 | 10.5448 | 72.9533 | 400.5999 | 0.01509413 | 79.7 | 34.51 | 0.58 |
| J101526-264259 | 764730 | 153.8614 | -26.7166 | 13.8652 | 47.6238 | 300.5138 | 0.03412958 | 213.3 | 36.64 | 0.58 |
| J101531-292423 | 29945 | 153.8793 | -29.4066 | 12.4099 | 66.2786 | 337.516 | 0.03173132 | 135.9 | 35.67 | 0.58 |
| J101537-272427 | - | 153.9057 | -27.4078 | 15.3554 | 49.2591 | 96.3481 | 0.01157047 | 49.1 | 33.46 | 0.58 |
| J101632-291258 | - | 154.1373 | -29.2163 | 13.0964 | 76.0108 | 176.2266 | 0.01514422 | 54.5 | 33.68 | 0.64 |
| J101756-285557 | - | 154.4866 | -28.9325 | 14.4099 | 67.8558 | 170.5825 | 0.03769535 | 93.8 | 34.86 | 0.58 |
| J101834-281550 | 3753792 | 154.6456 | -28.264 | 14.6891 | 47.6238 | 151.6106 | 0.04194573 | 85.3 | 34.65 | 0.59 |
| J101920-264135 | 30161 | 154.8353 | -26.6931 | 12.3029 | 56.6184 | 318.5536 | 0.04414246 | 116.0 | 35.32 | 0.58 |
| J101927-264159 | 764945 | 154.8662 | -26.6999 | 14.1879 | 50.3033 | 110.4705 | 0.00964968 | 37.2 | 32.85 | 0.58 |
| J102017-253913 | 30216 | 155.0743 | -25.6538 | 13.4071 | 51.6485 | 150.4681 | 0.01264661 | 46.6 | 33.34 | 0.58 |
| J102019-285220 | 30218 | 155.0828 | -28.8722 | 11.15 | 76.9694 | 429.0481 | 0.03237219 | 119.9 | 35.39 | 0.58 |
| J102023-253050 | - | 155.0966 | -25.514 | 15.3675 | 58.4722 | 132.569 | 0.01211333 | 90.4 | 34.78 | 0.58 |
| J102030-260951 | 30234 | 155.1281 | -26.1642 | 12.8541 | 48.6094 | 417.2113 | 0.0572516 | 249.2 | 36.98 | 0.58 |
| J102100-273339 | 753130 | 155.2535 | -27.5608 | 14.1518 | 55.7186 | 254.1508 | 0.03442685 | 177.2 | 36.24 | 0.58 |
| J102115-250342 | 783072 | 155.3137 | -25.0618 | 13.6738 | 52.5855 | 313.4991 | 0.03393395 | 211.6 | 36.63 | 0.58 |
| J102233-294017 | 726509 | 155.6378 | -29.6715 | 14.9756 | 47.6238 | 200.3425 | 0.02718859 | 165.0 | 36.09 | 0.58 |
| J102328-253424 | 777390 | 155.8685 | -25.5736 | 12.4153 | 68.5745 | 399.6161 | 0.04170041 | 187.7 | 36.37 | 0.58 |
| J102338-264531 | 764220 | 155.9116 | -26.7589 | 14.1452 | 53.9731 | 290.575 | 0.03581803 | 227.6 | 36.79 | 0.58 |
| J102416-270241 | 760541 | 156.0683 | -27.0448 | 14.424 | 47.4581 | 261.9494 | 0.03578983 | 212.7 | 36.64 | 0.58 |
| J102430-290904 | 732726 | 156.1259 | -29.1511 | 13.6075 | 54.5075 | 143.7009 | 0.01363351 | 46.8 | 33.35 | 0.58 |
| J102439-274841 | 749549 | 156.1626 | -27.8117 | 15.1621 | 49.5819 | 136.6024 | 0.01315652 | 87.1 | 34.7 | 0.58 |
| J102600-280334 | - | 156.5018 | -28.0597 | 15.2205 | 54.9633 | 173.4279 | 0.0375637 | 140.5 | 35.74 | 0.58 |
| J102621-291150 | 732211 | 156.5886 | -29.1973 | 13.6973 | 62.403 | 97.0405 | 0.01345127 | 23.2 | 31.83 | 0.58 |
| J102637-264142 | 764986 | 156.6545 | -26.6952 | 14.5557 | 57.7338 | 112.3494 | 0.0325455 | 45.5 | 33.29 | 0.59 |
| J102643-261256 | 770222 | 156.6797 | -26.2157 | 12.7449 | 51.6485 | 345.5666 | 0.03439577 | 165.9 | 36.1 | 0.58 |
| J102747-283425 | - | 156.9461 | -28.5738 | 15.4282 | 48.6909 | 238.2983 | 0.03272924 | 282.3 | 37.25 | 0.58 |
| J102818-255446 | 773700 | 157.0764 | -25.9129 | 16.0183 | 52.43 | 93.3625 | 0.01386497 | 62.8 | 33.99 | 0.58 |
| J102934-261937 | 30912 | 157.3949 | -26.3271 | 12.8164 | 47.2921 | 217.74 | 0.01427068 | 71.5 | 34.27 | 0.58 |
| J103002-284116 | 738653 | 157.5091 | -28.688 | 13.1147 | 61.3915 | 124.1583 | 0.01394284 | 28.3 | 32.26 | 0.58 |
| J103015-270743 | 759425 | 157.5651 | -27.1287 | 14.5215 | 69.0066 | 215.2906 | 0.03749136 | 153.4 | 35.93 | 0.58 |
| J103114-295837 | 722930 | 157.809 | -29.9771 | 14.6759 | 59.2068 | 109.4269 | 0.01511548 | 45.7 | 33.3 | 0.58 |
| J103139-273049 | 753808 | 157.9143 | -27.5138 | 14.3307 | 51.334 | 165.215 | 0.01305822 | 85.1 | 34.65 | 0.58 |
| J103141-300815 | 720959 | 157.921 | -30.1377 | 14.8566 | 62.8353 | 97.786 | 0.01849056 | 40.2 | 33.02 | 0.58 |
| J103240-282058 | 742765 | 158.169 | -28.3495 | 12.6848 | 71.4757 | 181.3984 | 0.01422809 | 47.6 | 33.39 | 0.58 |
| J103241-273137 | 31149 | 158.1721 | -27.5271 | 12.0583 | 71.4757 | 147.6499 | 0.01391053 | 24.2 | 31.91 | 0.58 |
| J103257-250937 | 782023 | 158.2381 | -25.1609 | 14.5155 | 62.1144 | 243.2447 | 0.02565921 | 192.8 | 36.43 | 0.62 |
| J103258-274013 | 31171 | 158.2426 | -27.6711 | 13.0522 | 70.8908 | 126.9981 | 0.01160875 | 28.7 | 32.29 | 0.58 |
| J103348-271429 | 757813 | 158.452 | -27.2417 | 13.1222 | 56.1694 | 346.7011 | 0.03655502 | 198.6 | 36.49 | 0.58 |
| J103353-274945 | 31238 | 158.4748 | -27.8291 | 12.2977 | 60.448 | 214.9652 | 0.01032262 | 54.9 | 33.7 | 0.58 |
| J103359-301003 | 31242 | 158.4966 | -30.1677 | 9.8673 | 78.7202 | 407.8787 | 0.01277512 | 60.3 | 33.9 | 0.58 |
| J103420-265408 | 92288 | 158.5865 | -26.9023 | 14.011 | 78.9802 | 135.4984 | 0.01362264 | 50.5 | 33.51 | 0.58 |
| J103502-293019 | 728536 | 158.7604 | -29.5062 | 12.3451 | 49.8231 | 111.2483 | 0.01362627 | 16.1 | 31.04 | 0.58 |
| J103507-275923 | 31334 | 158.783 | -27.9905 | 12.1861 | 73.7025 | 168.7821 | 0.00926373 | 33.0 | 32.59 | 0.58 |
| J103521-274137 | 31355 | 158.8391 | -27.6938 | 13.2414 | 75.6965 | 175.4385 | 0.01079559 | 57.7 | 33.81 | 0.58 |
| J103547-290131 | 31390 | 158.9463 | -29.0252 | 13.0973 | 50.2235 | 312.2781 | 0.03381084 | 161.0 | 36.03 | 0.58 |
| J103609-244856 | 31415 | 159.0412 | -24.8154 | 13.0609 | 53.8966 | 84.1631 | 0.00454496 | 13.2 | 30.61 | 0.58 |
| J103645-281010 | 744989 | 159.1902 | -28.1698 | 13.2636 | 49.0161 | 162.9367 | 0.01278334 | 50.7 | 33.53 | 0.58 |

Table A1 – continued

| Name | PGC | RA | DEC | Wl_{tot} | i | W_{mx} | z_{cmb} | d_L | μ | e_μ |
|----------------|---------|----------|-----------|-------------------|---------|-----------------|------------------|-------|-------|---------|
| J103646-293253 | 31484 | 159.196 | − 29.5482 | 13.2256 | 51.334 | 197.2334 | 0.01304613 | 71.5 | 34.27 | 0.58 |
| J103650-270902 | 31490 | 159.2096 | − 27.1485 | 13.177 | 67.8558 | 292.5814 | 0.03859519 | 147.7 | 35.85 | 0.58 |
| J103651-260227 | 31491 | 159.2131 | − 26.0412 | 13.526 | 49.8231 | 204.1734 | 0.00907223 | 87.7 | 34.72 | 0.58 |
| J103653-270311 | 31494 | 159.2211 | − 27.0532 | 12.0485 | 54.6596 | 234.1461 | 0.01299891 | 57.6 | 33.8 | 0.58 |
| J103655-265412 | 762452 | 159.233 | − 26.9029 | 13.0441 | 64.2723 | 199.8074 | 0.01197818 | 67.4 | 34.14 | 0.58 |
| J103701-284018 | 738882 | 159.2551 | − 28.6725 | 14.2125 | 65.4907 | 236.2912 | 0.03368768 | 158.7 | 36.0 | 0.58 |
| J103704-252038 | 31514 | 159.2683 | − 25.3441 | 12.3722 | 76.8078 | 199.2584 | 0.01353874 | 49.2 | 33.46 | 0.58 |
| J103737-261641 | 31574 | 159.4074 | − 26.2776 | 10.7246 | 53.0503 | 322.8375 | 0.01385994 | 57.5 | 33.8 | 0.58 |
| J103803-281007 | 31602 | 159.5132 | − 28.1688 | 14.1108 | 72.5815 | 304.9854 | 0.03634067 | 245.6 | 36.95 | 0.58 |
| J103809-260453 | 31612 | 159.5414 | − 26.0815 | 13.0599 | 72.73 | 144.5152 | 0.0130769 | 36.8 | 32.83 | 0.58 |
| J103818-285307 | 31626 | 159.5743 | − 28.8845 | 11.4949 | 74.69 | 297.56 | 0.01578427 | 70.3 | 34.23 | 0.58 |
| J103828-283056 | 740766 | 159.6196 | − 28.5157 | 13.8722 | 52.6631 | 169.7936 | 0.01568042 | 72.6 | 34.3 | 0.58 |
| J103840-283405 | 31642 | 159.6679 | − 28.5684 | 10.4866 | 64.4158 | 323.7424 | 0.01272478 | 51.8 | 33.57 | 0.58 |
| J103858-300500 | 3758554 | 159.7422 | − 30.084 | 15.1371 | 63.8418 | 81.3298 | 0.01370769 | 32.2 | 32.54 | 0.6 |
| J103902-291255 | 31664 | 159.7607 | − 29.2144 | 13.9916 | 62.6913 | 165.4385 | 0.01181481 | 73.0 | 34.32 | 0.58 |
| J103905-265519 | 93061 | 159.7724 | − 26.9228 | 12.8866 | 66.2069 | 350.8164 | 0.0363276 | 182.2 | 36.3 | 0.58 |
| J103918-265030 | 31683 | 159.8261 | − 26.8421 | 10.3241 | 72.1376 | 344.6117 | 0.01142924 | 54.1 | 33.67 | 0.58 |
| J103922-293505 | 31690 | 159.8422 | − 29.5846 | 11.6635 | 48.8537 | 274.8887 | 0.01408946 | 65.4 | 34.08 | 0.58 |
| J104000-292445 | 31732 | 160.0014 | − 29.4123 | 13.127 | 66.3502 | 184.4949 | 0.01371067 | 60.3 | 33.9 | 0.58 |
| J104004-301606 | 31738 | 160.0178 | − 30.2679 | 10.59 | 65.634 | 286.5209 | 0.01248467 | 43.1 | 33.17 | 0.58 |
| J104058-274546 | 750199 | 160.2427 | − 27.7623 | 14.349 | 67.1384 | 162.7876 | 0.01446573 | 83.4 | 34.61 | 0.58 |
| J104059-270456 | 31805 | 160.2475 | − 27.0819 | 9.6466 | 56.2443 | 396.914 | 0.01698876 | 51.8 | 33.57 | 0.58 |
| J104100-284430 | 31809 | 160.2552 | − 28.7418 | 12.2681 | 55.5679 | 192.7746 | 0.01365658 | 44.1 | 33.22 | 0.58 |
| J104139-254049 | – | 160.4145 | − 25.6805 | 14.4528 | 54.6596 | 122.5896 | 0.01404383 | 51.2 | 33.54 | 0.58 |
| J104139-274639 | 31852 | 160.4136 | − 27.778 | 13.753 | 59.865 | 136.4406 | 0.01569824 | 45.4 | 33.28 | 0.58 |
| J104157-264302 | – | 160.4888 | − 26.7174 | 13.6008 | 63.4108 | 256.0838 | 0.03786389 | 139.5 | 35.72 | 0.58 |
| J104239-300357 | – | 160.6646 | − 30.0664 | 15.6547 | 69.6565 | 82.1224 | 0.00940569 | 41.7 | 33.1 | 0.6 |
| J104245-264738 | 31924 | 160.6913 | − 26.7937 | 12.522 | 57.7338 | 345.3264 | 0.03673843 | 149.5 | 35.87 | 0.58 |
| J104252-252014 | – | 160.7192 | − 25.3373 | 13.8052 | 48.935 | 126.0006 | 0.02245921 | 40.0 | 33.01 | 0.58 |
| J104311-261500 | 31951 | 160.7974 | − 26.2501 | 10.1873 | 61.1016 | 430.6217 | 0.01629157 | 77.5 | 34.45 | 0.58 |
| J104326-251857 | 31960 | 160.859 | − 25.316 | 13.5057 | 48.6094 | 125.2967 | 0.01373015 | 34.5 | 32.69 | 0.58 |
| J104339-285157 | 31981 | 160.913 | − 28.8661 | 10.9693 | 76.7273 | 283.5747 | 0.01271548 | 50.4 | 33.51 | 0.58 |
| J104414-271548 | 757564 | 161.0589 | − 27.2637 | 14.1818 | 59.1335 | 226.0111 | 0.03779767 | 143.8 | 35.79 | 0.58 |
| J104442-290119 | 734399 | 161.1761 | − 29.0214 | 15.2513 | 59.1335 | 137.4706 | 0.03477507 | 91.8 | 34.81 | 0.58 |
| J104524-251723 | 780619 | 161.3536 | − 25.2898 | 13.9341 | 50.9391 | 271.7404 | 0.04946774 | 181.9 | 36.3 | 0.58 |
| J104620-293733 | 727073 | 161.586 | − 29.626 | 13.0861 | 56.9913 | 269.5008 | 0.04061149 | 121.2 | 35.42 | 0.58 |
| J104629-253308 | 32175 | 161.6229 | − 25.5523 | 14.8472 | 65.7056 | 145.9224 | 0.01318261 | 85.3 | 34.66 | 0.59 |

Table A2. Norma H I data from WALLABY phase 1 pilot survey.

| Name | PGC | RA | DEC | W_{tot} | i | W_{mx} | z_{cmb} | d_L | μ | e_μ |
|----------------|---------|------------|------------|------------------|---------|-----------------|------------------|-------|-------|---------|
| J163435-620248 | 58527 | 248.647418 | -62.046778 | 12.5906 | 62.8353 | 234.9112 | 0.01511102 | 74.4 | 34.36 | 0.58 |
| J163749-621352 | 4077297 | 249.454206 | -62.231162 | 10.5802 | 54.7356 | 175.1385 | 0.01625367 | 16.9 | 31.14 | 0.58 |
| J163927-594844 | 3078607 | 249.866523 | -59.812295 | 12.0403 | 67.2818 | 471.588 | 0.03785902 | 216.1 | 36.67 | 0.58 |
| J164107-605902 | 58755 | 250.281497 | -60.983986 | 13.5023 | 80.7086 | 160.1005 | 0.01186631 | 54.7 | 33.69 | 0.59 |
| J164113-603202 | - | 250.307194 | -60.534109 | 13.7705 | 56.9913 | 186.0271 | 0.03986854 | 82.3 | 34.58 | 0.58 |
| J164206-613441 | 3078658 | 250.528374 | -61.578262 | 14.1884 | 71.4757 | 191.9448 | 0.01770498 | 105.9 | 35.12 | 0.58 |
| J164249-610527 | 92488 | 250.707724 | -61.091025 | 10.6964 | 79.8702 | 310.8455 | 0.01506462 | 52.8 | 33.61 | 0.58 |
| J164355-620233 | 349886 | 250.981502 | -62.042582 | 12.6012 | 52.973 | 379.5319 | 0.03933249 | 185.4 | 36.34 | 0.58 |
| J164437-605103 | 58893 | 251.156286 | -60.851094 | 10.5273 | 72.0638 | 424.6372 | 0.01781932 | 88.3 | 34.73 | 0.58 |
| J164455-575030 | 3078727 | 251.230899 | -57.841714 | 12.282 | 47.209 | 400.6343 | 0.04826815 | 177.3 | 36.24 | 0.58 |
| J164508-611614 | - | 251.285273 | -61.27071 | 13.1157 | 79.3316 | 171.9725 | 0.01246623 | 52.5 | 33.6 | 0.58 |
| J164727-575143 | 3078771 | 251.863957 | -57.862209 | 13.2117 | 62.8353 | 361.9206 | 0.04771013 | 224.5 | 36.76 | 0.58 |
| J164739-570817 | 393557 | 251.914425 | -57.138085 | 14.3561 | 54.7356 | 83.2827 | 0.00287685 | 23.5 | 31.86 | 0.59 |
| J164749-613936 | - | 251.954282 | -61.660226 | 12.805 | 63.5545 | 174.2319 | 0.01770366 | 46.6 | 33.34 | 0.58 |
| J164826-623040 | 343635 | 252.108723 | -62.511225 | 11.9037 | 62.8353 | 185.4562 | 0.01496239 | 34.6 | 32.7 | 0.58 |
| J164911-620001 | 350325 | 252.298069 | -62.000386 | 12.6063 | 57.7338 | 275.5516 | 0.05177993 | 101.3 | 35.03 | 0.58 |
| J165131-603514 | 59130 | 252.882699 | -60.587289 | 12.5929 | 64.9176 | 133.5985 | 0.01132893 | 25.6 | 32.04 | 0.58 |
| J165439-605730 | - | 253.663341 | -60.95855 | 14.0336 | 69.2952 | 168.9091 | 0.01054331 | 77.4 | 34.44 | 0.58 |
| J165455-610856 | 357773 | 253.730344 | -61.149002 | 15.647 | 54.7356 | 105.3281 | 0.01482964 | 66.5 | 34.11 | 0.59 |
| J165520-592615 | 3078940 | 253.834941 | -59.437529 | 13.5311 | 75.2293 | 153.058 | 0.01655333 | 50.9 | 33.54 | 0.58 |
| J165559-592439 | 165948 | 253.997339 | -59.410888 | 11.7775 | 47.6238 | 265.3185 | 0.01615457 | 64.4 | 34.04 | 0.58 |
| J165632-594959 | 4584387 | 254.134589 | -59.833236 | 11.8378 | 54.5836 | 468.7337 | 0.04802051 | 194.6 | 36.45 | 0.58 |
| J165644-622413 | 4075676 | 254.184255 | -62.403763 | 9.9351 | 64.3441 | 377.1867 | 0.01719366 | 53.7 | 33.65 | 0.58 |
| J165645-620555 | - | 254.191411 | -62.098772 | 15.3289 | 58.4722 | 195.9205 | 0.03011796 | 186.1 | 36.35 | 0.59 |
| J165840-582909 | 141869 | 254.669097 | -58.485927 | 11.0622 | 54.7356 | 307.411 | 0.02063727 | 61.2 | 33.93 | 0.58 |
| J165847-612501 | - | 254.69821 | -61.416959 | 14.2337 | 74.4606 | 160.8808 | 0.01597719 | 77.4 | 34.44 | 0.59 |
| J165934-623256 | 4080474 | 254.894684 | -62.548998 | 10.5454 | 57.1401 | 255.9524 | 0.01642583 | 34.1 | 32.66 | 0.58 |
| J170039-584218 | 377019 | 255.16626 | -58.705246 | 13.4896 | 69.2952 | 183.8757 | 0.02094197 | 70.8 | 34.25 | 0.59 |
| J170116-621215 | 165971 | 255.317106 | -62.204321 | 12.073 | 55.039 | 406.3242 | 0.04637359 | 165.4 | 36.09 | 0.58 |
| J170149-603901 | 165952 | 255.455525 | -60.650362 | 12.2495 | 65.3475 | 290.4757 | 0.01649612 | 95.0 | 34.89 | 0.58 |
| J170232-584322 | 165953 | 255.634453 | -58.722864 | 11.5633 | 60.1568 | 314.7373 | 0.02064314 | 80.6 | 34.53 | 0.58 |
| J170349-595038 | - | 255.954693 | -59.844105 | 13.0267 | 49.0161 | 253.0155 | 0.01982964 | 104.6 | 35.1 | 1.1 |
| J170700-600654 | 165955 | 256.751847 | -60.11503 | 12.2699 | 62.1144 | 227.4055 | 0.01436001 | 60.3 | 33.9 | 0.58 |
| J170747-595059 | 59659 | 256.947861 | -59.849852 | 11.7537 | 79.1552 | 281.0189 | 0.01579552 | 71.0 | 34.26 | 0.58 |
| J171120-603454 | 362143 | 257.833867 | -60.581908 | 14.2512 | 50.0636 | 95.2061 | 0.01670085 | 28.9 | 32.3 | 0.58 |
| J171134-610802 | - | 257.893397 | -61.134105 | 16.0695 | 54.7356 | 97.9796 | 0.00902464 | 70.5 | 34.24 | 0.6 |
| J171309-603124 | 362690 | 258.287752 | -60.523391 | 13.4709 | 70.4539 | 125.2158 | 0.01621556 | 33.9 | 32.65 | 0.58 |
| J171339-615822 | 92494 | 258.415875 | -61.973005 | 15.4747 | 64.2723 | 152.0756 | 0.01505209 | 123.2 | 35.45 | 0.59 |
| J171538-602409 | - | 258.909689 | -60.402582 | 13.0023 | 79.9614 | 243.7314 | 0.0195147 | 96.4 | 34.92 | 0.58 |
| J171558-590923 | - | 258.994367 | -59.156581 | 13.0923 | 72.0638 | 189.1948 | 0.01186545 | 62.2 | 33.97 | 0.58 |
| J171850-601104 | 365445 | 259.711772 | -60.184587 | 13.7175 | 47.1257 | 253.8042 | 0.01551251 | 144.7 | 35.8 | 0.58 |
| J171924-615016 | 92496 | 259.853206 | -61.837997 | 13.265 | 75.2293 | 276.1248 | 0.02455815 | 137.8 | 35.7 | 0.58 |

Table A3. Eridanus H I data from WALLABY phase 1 pilot survey.

| Name | PGC | RA | DEC | W_{tot} | i | W_{mx} | z_{cmb} | d_L | μ | e_μ |
|----------------|--------|-----------|------------|------------------|---------|-----------------|------------------|-------|-------|---------|
| J034114-235017 | 13561 | 55.308333 | -23.838056 | 10.1562 | 51.4127 | 254.5868 | 0.00591068 | 28.2 | 32.25 | 0.58 |
| J033859-223502 | 13442 | 54.745833 | -22.583889 | 13.3234 | 62.5472 | 171.2887 | 0.01408583 | 57.3 | 33.79 | 0.58 |
| J034056-223350 | 13544 | 55.233333 | -22.563889 | 8.0092 | 64.7743 | 374.7365 | 0.00478841 | 21.8 | 31.7 | 0.58 |
| J034517-230001 | 13760 | 56.320833 | -23.000278 | 9.306 | 56.1694 | 361.1469 | 0.00483078 | 37.0 | 32.84 | 0.58 |
| J034219-224520 | 13608 | 55.579167 | -22.755556 | 11.9271 | 51.6485 | 145.3675 | 0.00485579 | 22.1 | 31.72 | 0.58 |
| J033941-235054 | 13477 | 54.920833 | -23.848333 | 13.8833 | 82.0066 | 71.6966 | 0.00503014 | 14.2 | 30.77 | 0.58 |
| J034057-214245 | 13543 | 55.2375 | -21.7125 | 11.5644 | 74.9975 | 148.0462 | 0.00527728 | 19.3 | 31.43 | 0.58 |
| J034040-221711 | 13531 | 55.166667 | -22.286389 | 12.4245 | 77.6238 | 154.5925 | 0.00553255 | 31.2 | 32.47 | 0.58 |
| J034002-192200 | 13491 | 55.008333 | -19.366667 | 12.0881 | 80.6134 | 114.5336 | 0.00365656 | 15.1 | 30.9 | 0.58 |
| J034814-212824 | 13871 | 57.058333 | -21.473333 | 9.6576 | 55.1904 | 274.0381 | 0.00493632 | 25.8 | 32.06 | 0.58 |
| J034337-211418 | 13689 | 55.904167 | -21.238333 | 12.4218 | 72.5815 | 128.9114 | 0.00499355 | 22.1 | 31.72 | 0.58 |
| J034434-211123 | 135119 | 56.141667 | -21.189722 | 13.1936 | 70.0185 | 72.3556 | 0.00488434 | 10.6 | 30.12 | 0.58 |
| J034131-214051 | 13569 | 55.379167 | -21.680833 | 10.3246 | 74.4606 | 157.7669 | 0.00506959 | 12.3 | 30.45 | 0.58 |
| J033921-212450 | 13460 | 54.8375 | -21.413889 | 11.9631 | 66.4218 | 117.8377 | 0.00503156 | 15.1 | 30.89 | 0.58 |
| J033537-211742 | 13283 | 53.904167 | -21.295 | 11.8244 | 75.2293 | 146.8529 | 0.00562052 | 21.5 | 31.66 | 0.58 |
| J033341-212844 | 13184 | 53.420833 | -21.478889 | 8.9854 | 48.6094 | 265.2557 | 0.00578946 | 17.8 | 31.25 | 0.58 |
| J033347-192946 | 13190 | 53.445833 | -19.496111 | 10.187 | 54.7356 | 231.4768 | 0.00615231 | 23.9 | 31.89 | 0.58 |
| J033810-194412 | 13401 | 54.541667 | -19.736667 | 12.6368 | 71.7693 | 175.8256 | 0.01352603 | 43.9 | 33.21 | 0.58 |
| J033757-213938 | 13392 | 54.4875 | -21.660556 | 13.5581 | 73.552 | 136.5896 | 0.01347565 | 41.6 | 33.09 | 0.58 |
| J033147-211309 | 831121 | 52.945833 | -21.219167 | 14.354 | 64.9892 | 101.5197 | 0.01371815 | 34.2 | 32.67 | 0.58 |
| J032455-214701 | 12762 | 51.229167 | -21.783611 | 12.8097 | 55.1904 | 102.3076 | 0.00439474 | 17.0 | 31.16 | 0.58 |
| J032425-213233 | 12737 | 51.104167 | -21.5425 | 8.4969 | 72.5815 | 341.6675 | 0.00484116 | 23.0 | 31.8 | 0.58 |
| J033527-211302 | 831168 | 53.8625 | -21.217222 | 12.8515 | 48.4461 | 120.2676 | 0.00466241 | 23.6 | 31.86 | 0.58 |
| J032735-211339 | 12889 | 51.895833 | -21.2275 | 11.3398 | 75.7749 | 166.0928 | 0.00517694 | 21.7 | 31.68 | 0.58 |
| J032831-222957 | 813307 | 52.129167 | -22.499167 | 13.6391 | 73.7025 | 69.8049 | 0.00548873 | 12.1 | 30.41 | 0.58 |
| J033653-245445 | 13342 | 54.220833 | -24.9125 | 12.2326 | 58.3248 | 124.5537 | 0.00575066 | 19.0 | 31.39 | 0.58 |
| J033302-240756 | 13154 | 53.258333 | -24.132222 | 12.6236 | 71.4757 | 162.4149 | 0.00598226 | 37.5 | 32.87 | 0.58 |
| J033617-253615 | 13304 | 54.070833 | -25.604167 | 11.4992 | 67.3535 | 124.6075 | 0.00493199 | 13.5 | 30.66 | 0.58 |
| J032937-232103 | 12986 | 52.404167 | -23.350833 | 12.9769 | 74.3844 | 116.2925 | 0.00509535 | 23.5 | 31.85 | 0.58 |
| J033326-234246 | 13171 | 53.358333 | -23.712778 | 9.5617 | 76.0108 | 256.6107 | 0.00564806 | 21.8 | 31.69 | 0.58 |
| J033228-232245 | 13127 | 53.116667 | -23.379167 | 13.3847 | 56.3192 | 69.6998 | 0.00543831 | 10.7 | 30.15 | 0.58 |

Table A4. NGC4636 H I data from WALLABY phase 1 pilot survey.

| Name | PGC | RA | DEC | W_{tot} | i | W_{mx} | z_{cmb} | d_L | μ | e_μ |
|----------------|---------|-----------|----------|------------------|---------|-----------------|------------------|-------|-------|---------|
| J122708+055255 | 40801 | 186.78688 | 5.88209 | 10.7665 | 80.2379 | 166.4096 | 0.00485391 | 16.7 | 31.12 | 0.58 |
| J122713-020236 | 40820 | 186.8062 | -2.04356 | 11.9998 | 64.9892 | 82.7606 | 0.02268628 | 7.9 | 29.48 | 0.58 |
| J122729+073841 | 40861 | 186.87277 | 7.64494 | 12.0952 | 58.1773 | 141.229 | 0.00401966 | 22.6 | 31.77 | 0.58 |
| J122745+013601 | 135803 | 186.93906 | 1.60045 | 15.007 | 48.4461 | 66.8153 | 0.00548086 | 20.9 | 31.6 | 0.6 |
| J122755+054312 | 40933 | 186.9813 | 5.72019 | 11.3223 | 77.0504 | 138.523 | 0.00864351 | 15.3 | 30.92 | 0.58 |
| J122852+041739 | 41088 | 187.21861 | 4.2942 | 11.4152 | 81.1938 | 289.4117 | 0.01528698 | 64.3 | 34.04 | 0.58 |
| J122930+074142 | 41170 | 187.37658 | 7.69522 | 10.983 | 67.2818 | 190.8034 | 0.00363512 | 23.9 | 31.89 | 0.58 |
| J122932+005020 | 41177 | 187.38499 | 0.83914 | 14.2449 | 74.537 | 121.3941 | 0.00862244 | 45.6 | 33.3 | 0.58 |
| J123021-013813 | 3294304 | 187.59016 | -1.63716 | 15.4059 | 59.5728 | 73.0627 | 0.00827984 | 29.8 | 32.37 | 0.59 |
| J123022+034431 | 41307 | 187.59204 | 3.74218 | 10.8261 | 77.6238 | 317.3754 | 0.01525979 | 58.3 | 33.83 | 0.58 |
| J123026+041450 | 41317 | 187.61136 | 4.24724 | 9.5804 | 53.5128 | 385.5769 | 0.01525759 | 47.5 | 33.38 | 0.58 |
| J123132+071828 | 5060276 | 187.88433 | 7.30778 | 13.6058 | 70.0185 | 181.9531 | 0.02554986 | 73.2 | 34.32 | 0.58 |
| J123156+035316 | 97234 | 187.98655 | 3.88782 | 13.6432 | 59.2068 | 166.4686 | 0.01613459 | 62.9 | 33.99 | 0.58 |
| J123209-010543 | 1126897 | 188.04071 | -1.0955 | 14.2598 | 68.0712 | 130.4373 | 0.00917699 | 52.6 | 33.61 | 0.58 |
| J123228+002315 | 4105156 | 188.11709 | 0.38769 | 10.06 | 58.6929 | 170.8812 | 0.00624733 | 12.7 | 30.52 | 0.58 |
| J123236+023943 | 41599 | 188.15304 | 2.66221 | 11.4103 | 74.4606 | 142.1978 | 0.00693114 | 16.7 | 31.11 | 0.58 |
| J123244+000656 | 41618 | 188.18667 | 0.11568 | 7.074 | 83.1277 | 303.1783 | 0.00490181 | 9.5 | 29.89 | 0.58 |
| J123249+031748 | 41625 | 188.20644 | 3.2967 | 12.0076 | 52.43 | 240.9763 | 0.01779495 | 59.7 | 33.88 | 0.58 |
| J123250+054744 | 41627 | 188.21004 | 5.79565 | 12.6288 | 47.6238 | 282.9161 | 0.04053226 | 107.6 | 35.16 | 0.58 |
| J123257+043441 | 41647 | 188.23937 | 4.57811 | 13.5008 | 61.6809 | 80.6525 | 0.00524331 | 14.9 | 30.87 | 0.58 |
| J123320+013119 | 41700 | 188.33727 | 1.522 | 12.8429 | 66.78 | 72.9055 | 0.00672987 | 9.1 | 29.8 | 0.58 |
| J123329+034732 | 41716 | 188.37108 | 3.79235 | 12.5449 | 55.8691 | 103.8952 | 0.00414349 | 15.5 | 30.96 | 0.58 |
| J123407+023905 | 6656564 | 188.53133 | 2.65142 | 6.664 | 77.7896 | 363.2169 | 0.00692832 | 11.1 | 30.22 | 0.58 |
| J123422+021914 | 41816 | 188.59283 | 2.32075 | 10.8866 | 78.8932 | 116.176 | 0.00703584 | 8.9 | 29.76 | 0.58 |
| J123427+021108 | 41823 | 188.61479 | 2.18573 | 7.1732 | 70.1635 | 332.7434 | 0.00715977 | 11.9 | 30.37 | 0.58 |
| J123554-015112 | 41998 | 188.97833 | -1.85339 | 12.6614 | 54.8115 | 264.2974 | 0.02412559 | 96.1 | 34.91 | 0.58 |
| J123555-025405 | 41982 | 188.9812 | -2.90157 | 11.45 | 50.9391 | 315.5279 | 0.0249257 | 76.9 | 34.43 | 0.58 |
| J123609+073152 | 1324268 | 189.03896 | 7.53129 | 11.8096 | 48.4461 | 363.4753 | 0.0251558 | 118.6 | 35.37 | 0.58 |
| J123630+001315 | 1160233 | 189.12733 | 0.22084 | 13.7662 | 52.5855 | 171.2284 | 0.01355351 | 70.2 | 34.23 | 0.58 |
| J123641+030621 | 42080 | 189.17337 | 3.10604 | 13.3826 | 67.8558 | 129.5563 | 0.0059399 | 34.7 | 32.7 | 0.58 |
| J123651-003515 | 1139671 | 189.21624 | -0.58766 | 14.973 | 50.4627 | 70.0198 | 0.00971782 | 22.5 | 31.76 | 0.58 |
| J123703+065533 | 42108 | 189.26346 | 6.92604 | 11.675 | 55.1147 | 101.1826 | 0.00658373 | 9.9 | 29.98 | 0.58 |
| J123734+042150 | 42152 | 189.3924 | 4.36412 | 10.6519 | 56.693 | 204.6089 | 0.01881 | 23.4 | 31.85 | 0.58 |
| J123742-033505 | 42153 | 189.42797 | -3.58497 | 16.4708 | 62.1144 | 75.8018 | 0.02525376 | 52.1 | 33.59 | 0.6 |
| J123748-012038 | 42173 | 189.45018 | -1.34409 | 12.8769 | 51.1762 | 68.0291 | 0.00629811 | 8.1 | 29.55 | 0.58 |
| J123802+001036 | 1159012 | 189.51118 | 0.17674 | 14.8585 | 46.8753 | 139.7513 | 0.01457574 | 79.0 | 34.49 | 0.58 |
| J123805-000137 | 42202 | 189.52254 | -0.027 | 10.6346 | 64.7026 | 343.9878 | 0.01365786 | 62.2 | 33.97 | 0.58 |
| J123805-002419 | 1144183 | 189.52404 | -0.40528 | 14.7913 | 75.3069 | 185.0515 | 0.02660916 | 130.4 | 35.58 | 0.61 |
| J123827+041912 | 42241 | 189.61541 | 4.31999 | 8.4081 | 71.4757 | 255.2234 | 0.00376112 | 12.7 | 30.52 | 0.58 |
| J123835+012413 | 42255 | 189.64817 | 1.40361 | 11.7301 | 76.4072 | 292.1839 | 0.01848818 | 75.6 | 34.39 | 0.58 |
| J123912+060038 | 42319 | 189.80195 | 6.01063 | 10.0503 | 55.6433 | 350.0738 | 0.00921195 | 49.1 | 33.46 | 0.58 |
| J123917-003149 | 42336 | 189.82234 | -0.5305 | 9.3979 | 73.7025 | 201.0799 | 0.00470376 | 12.7 | 30.52 | 0.58 |
| J123922+045608 | 42340 | 189.84246 | 4.93578 | 12.2544 | 48.6094 | 113.3002 | 0.00651829 | 16.0 | 31.02 | 0.58 |
| J123928+041549 | 42354 | 189.8694 | 4.26381 | 12.241 | 70.0185 | 277.7179 | 0.05026681 | 86.9 | 34.7 | 0.58 |
| J123949+014016 | 42393 | 189.95774 | 1.67115 | 11.9926 | 62.0422 | 107.552 | 0.00521402 | 12.9 | 30.55 | 0.58 |
| J124002-010258 | 1128047 | 190.01187 | -1.04943 | 13.3498 | 65.0609 | 77.1982 | 0.00646665 | 12.8 | 30.54 | 0.58 |
| J124002-033623 | 42409 | 190.00896 | -3.60656 | 13.5385 | 59.938 | 114.3869 | 0.00962714 | 29.4 | 32.35 | 0.58 |
| J124109+041725 | 1266160 | 190.28802 | 4.2904 | 14.3298 | 78.463 | 99.0002 | 0.02999321 | 32.2 | 32.54 | 0.59 |
| J124111-013526 | 42538 | 190.29587 | -1.59063 | 12.8232 | 60.9566 | 205.8903 | 0.0144801 | 64.5 | 34.05 | 0.58 |
| J124111+012435 | 42542 | 190.29831 | 1.40986 | 11.6131 | 51.57 | 211.9055 | 0.00680496 | 39.0 | 32.96 | 0.58 |
| J124121+001315 | 1160198 | 190.34052 | 0.22109 | 15.404 | 64.7026 | 141.577 | 0.01714687 | 104.1 | 35.09 | 0.62 |
| J124123-030327 | 42559 | 190.34617 | -3.0577 | 11.5192 | 65.9205 | 98.5783 | 0.00597682 | 8.8 | 29.71 | 0.58 |
| J124128-031517 | 91219 | 190.36976 | -3.25471 | 14.7345 | 72.5815 | 111.0944 | 0.00714245 | 48.3 | 33.42 | 0.58 |
| J124232-000459 | 42689 | 190.63607 | -0.08324 | 8.7895 | 64.4158 | 239.4807 | 0.00687653 | 13.4 | 30.64 | 0.58 |
| J124237-020708 | 3106365 | 190.65649 | -2.11895 | 14.4447 | 48.4461 | 265.9249 | 0.04714775 | 220.9 | 36.72 | 0.58 |
| J124240+012047 | 42709 | 190.66927 | 1.34646 | 11.0747 | 53.5128 | 325.8747 | 0.01788554 | 68.8 | 34.19 | 0.58 |
| J124257-011345 | 42747 | 190.73947 | -1.22941 | 10.3528 | 76.647 | 315.5301 | 0.01184754 | 46.4 | 33.33 | 0.58 |
| J124317-003841 | 42791 | 190.82337 | -0.64492 | 10.2494 | 72.2114 | 303.5107 | 0.00996205 | 41.1 | 33.07 | 0.58 |
| J124333+014827 | 92947 | 190.88767 | 1.8077 | 12.2973 | 61.6086 | 173.919 | 0.04960635 | 36.8 | 32.83 | 0.58 |
| J124350-003344 | 42847 | 190.96079 | -0.56243 | 9.5363 | 48.4461 | 265.9249 | 0.00990722 | 23.0 | 31.81 | 0.58 |
| J124421+042536 | 42892 | 191.08944 | 4.42672 | 12.0215 | 60.6661 | 303.9758 | 0.02972201 | 93.2 | 34.85 | 0.58 |
| J124428-030017 | 42909 | 191.11791 | -3.0048 | 11.1596 | 49.7428 | 453.3832 | 0.02503503 | 133.7 | 35.63 | 0.58 |
| J124428+002815 | 42910 | 191.119 | 0.47091 | 10.9498 | 79.3316 | 103.7941 | 0.00506443 | 7.4 | 29.36 | 0.58 |
| J124433-021916 | 42921 | 191.14097 | -2.32119 | 12.8803 | 55.1904 | 133.9742 | 0.00643985 | 29.3 | 32.34 | 0.58 |
| J124508-002747 | 42975 | 191.28452 | -0.46322 | 6.6948 | 66.1353 | 422.087 | 0.00619415 | 14.9 | 30.87 | 0.58 |

Table A4 – continued

| Name | PGC | RA | DEC | W_{tot} | i | W_{mx} | z_{cmb} | d_L | μ | e_μ |
|----------------|---------|-----------|----------|------------------|---------|-----------------|------------------|-------|-------|---------|
| J124531-003203 | 3110155 | 191.38242 | -0.53434 | 10.5016 | 58.0296 | 157.9589 | 0.00652746 | 13.4 | 30.64 | 0.58 |
| J124548-002600 | 1143451 | 191.45039 | -0.43347 | 13.7782 | 53.6665 | 74.4803 | 0.00670022 | 14.6 | 30.82 | 0.58 |
| J124608+042643 | 1268285 | 191.53441 | 4.4453 | 13.9988 | 65.8488 | 229.0488 | 0.02473573 | 135.6 | 35.66 | 0.58 |
| J124645+055723 | 43106 | 191.69058 | 5.95643 | 10.8463 | 55.9442 | 143.6344 | 0.0038936 | 13.1 | 30.59 | 0.58 |
| J124651-013308 | 3295908 | 191.71291 | -1.55242 | 14.837 | 56.7677 | 69.3402 | 0.02402866 | 20.8 | 31.59 | 0.59 |
| J124701-013444 | 43128 | 191.75426 | -1.57889 | 12.1334 | 49.8231 | 198.9382 | 0.01021996 | 44.0 | 33.22 | 0.58 |
| J124717+002405 | 43153 | 191.82103 | 0.40156 | 11.0785 | 60.6661 | 156.0027 | 0.04758206 | 17.1 | 31.16 | 0.58 |
| J124753-011107 | 43198 | 191.97243 | -1.18529 | 11.8646 | 69.8012 | 349.4939 | 0.02458987 | 113.0 | 35.26 | 0.58 |
| J124800+042609 | 3994854 | 192.0002 | 4.43583 | 12.4899 | 56.2443 | 155.1573 | 0.00450877 | 32.4 | 32.55 | 0.58 |
| J125038+012749 | 43470 | 192.66139 | 1.46365 | 10.874 | 79.7794 | 175.7894 | 0.00535511 | 19.5 | 31.45 | 0.58 |
| J124808+033759 | 5808028 | 192.03338 | 3.63328 | 14.7059 | 54.7356 | 93.0806 | 0.02466785 | 34.1 | 32.67 | 0.7 |

¹University Lyon 1, IUF, IP2I Lyon, F-69622 Villeurbanne cedex, France²School of Mathematics and Physics, The University of Queensland, Brisbane, QLD 4072, Australia³Centre for Astrophysics, Supercomputing, Swinburne University, Hawthorn, VIC 3122, Australia⁴Astronomy Department, University of Cape Town, Private Bag X3, Rondebosch, 7701, South Africa⁵IRFU, CEA Université Paris-Saclay, F-91191 Gif-sur-Yvette, France⁶International Centre for Radio Astronomy Research (ICRAR), The University of Western Australia, M468, Crawley, WA 6009, Australia⁷ARC Centre of Excellence for Astrophysics in 3 Dimensions (ASTRO 3D), Stromlo, ACT 2611, Australia⁸Korea Institute for Advanced Study, 85, Hoegi-ro, Dongdaemun-gu, Seoul 02455, Republic of Korea⁹National Astronomical Observatories, Chinese Academy of Sciences, 20A Datun Road, Chaoyang District, Beijing 100012, China¹⁰Department of Physics, Engineering Physics and Astronomy Queen's University Kingston, ON K7L 3N6, Canada¹¹INAF - Osservatorio Astronomico di Cagliari, Via della Scienza 5, I-09047 Selargius, CA, Italy¹²Australia Telescope National Facility, CSIRO Astronomy and Space Science, PO Box 76, NSW 1710, Epping, Australia¹³Western Sydney University, Locked Bag 1797, Penrith, NSW 2751, Australia¹⁴CSIRO Space, Astronomy, PO Box 1130, Bentley, WA 6102, Australia¹⁵Royal Military College of Canada, PO Box 17000, Station Forces, Kingston, Ontario, K7K7B4, Canada¹⁶Kavli Institute for Astronomy and Astrophysics, Peking University, Beijing 100871, China¹⁷Argelander-Institut für Astronomie, Universität Bonn, Auf dem Hügel 71, D-53121 Bonn, Germany¹⁸Aix Marseille University, CNRS, CNES, LAM, F-13013 Marseille, France¹⁹Research School of Astronomy and Astrophysics, Australian National University, Canberra, ACT 2611, Australia²⁰Department of Physics and Astronomy, University of Louisville, 102 Natural Science Building, 40292 KY Louisville, USA²¹Special Astrophysical Observatory, Russian Academy of Sciences, Nizhny Arkhyz, 369167, Russia²²Department of Physics and Astronomy, Rutgers University, 136 Frelinghuysen Road, Piscataway, NJ 08854, USAThis paper has been typeset from a \TeX/L\TeX file prepared by the author.